Available online at www.CivileJournal.org

Civil Engineering Journal

(E-ISSN: 2476-3055; ISSN: 2676-6957)

Vol. 11, No. 01, January, 2025

Sluice Gate Operation and Managed Water Levels Improve Predicted Estuarine Lake Water Quality

Semin Kim [1*]

[1] *Department of Civil Engineering, Jeonbuk National University, Jeonju-si 54896, Jeollabuk-do, Republic of Korea.*

Received 19 July 2024; Revised 18 December 2024; Accepted 26 December 2024; Published 01 January 2025

Abstract

Saemangeum Lake, an artificial estuarine lake, suffers from a pollutant load from an upstream watershed that is insufficiently mitigated by current load reduction measures. However, no studies have reported simulated flow direction and velocity for a lake. This study aimed to present an alternative solution based on managing water levels and sluice gate operation. Data were collected on water quality, sluice gate operation, water levels, tidal currents, and flow velocities. Next, the inflow and outflow volumes through the sluice gates were calculated. The Delft3D model was applied to predict water quality in a number of simulated scenarios. Finally, streamline and vorticity were calculated to evaluate hydraulic phenomena, while the ecology-based seawater quality index was employed to evaluate water quality. Analysis of flow characteristics revealed a large-scale clockwise vortex formed in the area where the Mangyeong River meets one of the sluice gates. It revealed a two-layer circulation with different flows in the surface and bottom layers. Evaluation of predicted water quality showed that one-way circulation, alternated in 15-day cycles, significantly improved major water quality items at most stations. Collectively, these findings demonstrate the effect that gate operation and managed water levels can have on the water quality of estuarine lakes.

Keywords: Saemangeum Lake; Water Quality; Sluice Gate Operation; Managed Water Level; Delft3D Model; Estuarine Lake Management; Ecology-Based Seawater Quality Index.

1. Introduction

Estuaries play a very important role in material circulation by acting as corridors through which pollutants undergo the filtration process during movement from land to coast [1]. These processes include seawater dilution with freshwater, nutrient uptake and release by organisms in the estuary, metal desorption and adsorption by particulate materials, as well as elution and removal from sediment [2]. However, relatively no estuaries in Korea have retained their original form due to the construction of estuarine weirs and seawalls since the 1990s [3, 4].

Globally, approximately 800,000 artificial lakes and reservoirs have been created for flood control, irrigation, hydropower generation, and domestic water supply [5–7]. Artificial lakes constructed for such purposes reduce the flow velocity of water flowing into the catchment area and decrease turbidity and sedimentation of particulate materials, which can increase primary production from improved transparency [8]. Consequently, the lake undergoes a gradual environmental change, wherein the organic matter generated within the lake gradually supersedes that from external sources [9]. Increased retention time due to an increase in autochthonous algae and a decrease in flow velocity may reduce dissolved oxygen in bottom water layers due to the accumulation and decomposition of organic matter produced in excess within the lake or introduced from upstream. Such environmental changes in the water layer can affect the

* Corresponding author: semkim@jbnu.ac.kr

http://dx.doi.org/10.28991/CEJ-2025-011-01-015

© 2025 by the authors. Licensee C.E.J, Tehran, Iran. This article is an open access article distributed under the terms and conditions of the Creative Commons Attribution (CC-BY) license (http://creativecommons.org/licenses/by/4.0/).

carbon, nitrogen, and phosphorus biogeochemical cycles in the lake [10, 11]. However, spatially, water quality improvement is difficult as the self-purification capacity declines considerably due to the structural characteristics of most lakes, which often resemble closed or semi-closed water bodies [12].

For many countries, artificial lakes represent an economical and efficient water resource [13], making management of their water quality essential. Accordingly, sustainability must be achieved by acquiring and monitoring data and establishing alternatives. Although monitoring is a useful method for minimizing the uncertainty in results, the task of identifying water pollution solely based on monitoring data can be time-consuming and costly for large-capacity lakes with numerous water quality variables [14]. It is, therefore, necessary to build and operate water quality prediction models that can reasonably reproduce the mechanisms of a water body.

Given that the water within reservoirs is stagnant, its self-purifying ability is poorer than that of flowing water, with the organic matter deposited on the bottom decomposing and negatively impacting water quality [15]. Hence, studies have been performed in lakes where the water depth characteristics have a greater effect than the flow direction using three-dimensional models, including Delft3D [16–18], MIKE21 [19], Environmental Fluid Dynamics Code (EFDC) [20–25], and Generalized Environmental Modeling System for Surface waters (GEMSS) [26]. For example, Delft3D has been applied to simulate the water quality of Eğirdir Lake according to the amount of nonpoint source pollution load flowing into it. The validation items of the model include monthly water level and water temperature data [16]. The applicability of Delft3D using monitoring data has also been assessed for Hedberg Lake. Specifically, the model was validated for water level and water quality during the monsoon period (April–September); however, the water quality was validated using data for only 1 month [17]. Additionally, the Delft3D model was adopted to simulate the effect of hydraulic retention time (HRT) on water quality in Lake M—an artificial lake in China. Although the HRT impact was analyzed, only water quality was verified without confirming hydrodynamic data [18]. Meanwhile, the applicability of the MIKE21 model has been assessed in terms of the fluid dynamics and water quality in Manzala Lake; the model was verified using monthly water level, water temperature, and salinity data [19].

The EFDC model is a representative model used to study the fluid dynamics and water quality of lakes. This model has been applied to simulate the water level, COD, and NH3-N for Jingpo Lake in China [20]. It has also been used to assess water quality changes according to inflow and outflow in Yilong Lake; however, only water level data were verified [21]. Meanwhile, the impact of cyanobacteria on nitrogen (N) loading in Taihu Lake, China, was simulated without verifying the hydrodynamic model [22]. Additionally, research on Saemangeum Lake is underway using the EFDC model. For instance, Shin et al. [23] constructed an EFDC model and simulated water temperature and salinity to examine the reproducibility of the model. Subsequently, Cho et al. [24] quantitatively presented the influence range of sluice gate effluent through particle tracking experiments. Meanwhile, Kim et al. [25] improved the function of the EFDC model to dynamically control the benthic flux rate in the bottom layer of Saemangeum Lake, reporting excellent reproducibility. Additionally, Jeong et al. [26] successfully simulated changes in water temperature and salinity by combining the GEMSS—a three-dimensional water quality model—and the Hydrological Simulation Program FORTRAN (HSPF).

Although previous studies have provided valuable insights and strategies, the simulation periods related to hydrodynamics and water quality modeling rarely exceeded 12 months. Moreover, while the seasonal variation characteristics were simulated, hydrodynamic verification was only performed at the water level. Thus, given that the reproducibility of the water level data was only assessed using data measured at 1-month intervals, the fluid dynamic verification was insufficient. Additionally, no studies have reported simulated flow direction and velocity for a lake.

Saemangeum Lake continuously experiences various hydraulic and water quality issues throughout the year, including strong density stratification and two-layer circulation. To reproduce this phenomenon with a model, the depth grid configuration is critical. However, previous studies that have used EFDC have applied Sigma-layer, which is divided into the same number of layers in the depth direction. Therefore, as the thickness of the layer varies depending on the depth at each point, determining the flow characteristics at precise depths is challenging. Moreover, when applying sigma layers vertically, numerical errors may increase and density layer reproducibility may decrease. Meanwhile, the Delft3D model is a water quality model that includes flow/sedimentation (Delft3D-FLOW), wave (Delft3D-WAVE), and water quality (Delft3D-WAQ) modules. The Z-level of the Delft3D model has the same layer thickness throughout the entire section, facilitating the determination of flow characteristics at precise depths, with relatively high stratification reproducibility [27]. Many recent studies have applied the Delft3D model to evaluate the water quality of estuarine lakes [28–32].

To manage the water quality of Saemangeum Lake, the Korean government has been pursuing measures to reduce the pollutant load of the upstream watershed. However, a rising trend has been reported in the concentrations of water quality parameters in the downstream area [33], highlighting the limited water quality improvement achieved solely via load reduction. To analyze such a phenomenon, it is necessary to investigate the circulation and mass transfer characteristics. For improvement of water quality in estuarine lakes, structural and non-structural alternatives can be considered. Additionally, structural solutions are more time-consuming and costly than non-structural solutions, making

the latter an integral component of sustainable water quality improvement strategies for estuarine lakes. Bottom water drainage is a typical non-structural method that can improve the water quality of anoxic hypolimnion in stratified lakes [34]; however, in the absence of such systems, operating sluice gates can eliminate stagnant waters and induce water circulation.

The current study aimed to design an environmentally friendly and economical water quality management alternative solution for Saemangeum Lake water quality management using the Delft3D model. Hydraulic characteristics were analyzed by estimating streamline and vorticity, which affect the accumulation and retention time of materials. In addition, the ecology-based seawater quality index (ESWQI) was applied to analyze the water quality characteristics [33]. The characteristics of seawater inflow and outflow through sluice gates in Saemangeum Lake were considered key factors that influence the flow and material circulation, representing non-structural alternatives for water quality improvement. In addition, by monitoring the flow velocity and direction, fluid dynamics verification data were obtained and the reproducibility of the model was improved. Figure 1 presents the composition and input/output data of the hydrodynamic and water quality linkage models applied in this study.

The remainder of this article is structured as follows: (1) The amount of seawater inflow that can satisfy the target water quality of Saemangeum Lake was estimated, and a corresponding sluice gate operation scenario was developed. (2) Long-term precision monitoring of ungauged points was conducted to obtain high-resolution flow velocity test data, facilitating the establishment of highly reproducible Delft3D models. (3) The hydraulic characteristics, water quality characteristics, and water quality improvement effects were quantitatively evaluated by applying the sluice gate operation scenario. Collectively, the findings of this study can be applied to develop strategies for improving water quality by controlling the hydraulic phenomena in estuarine lakes.

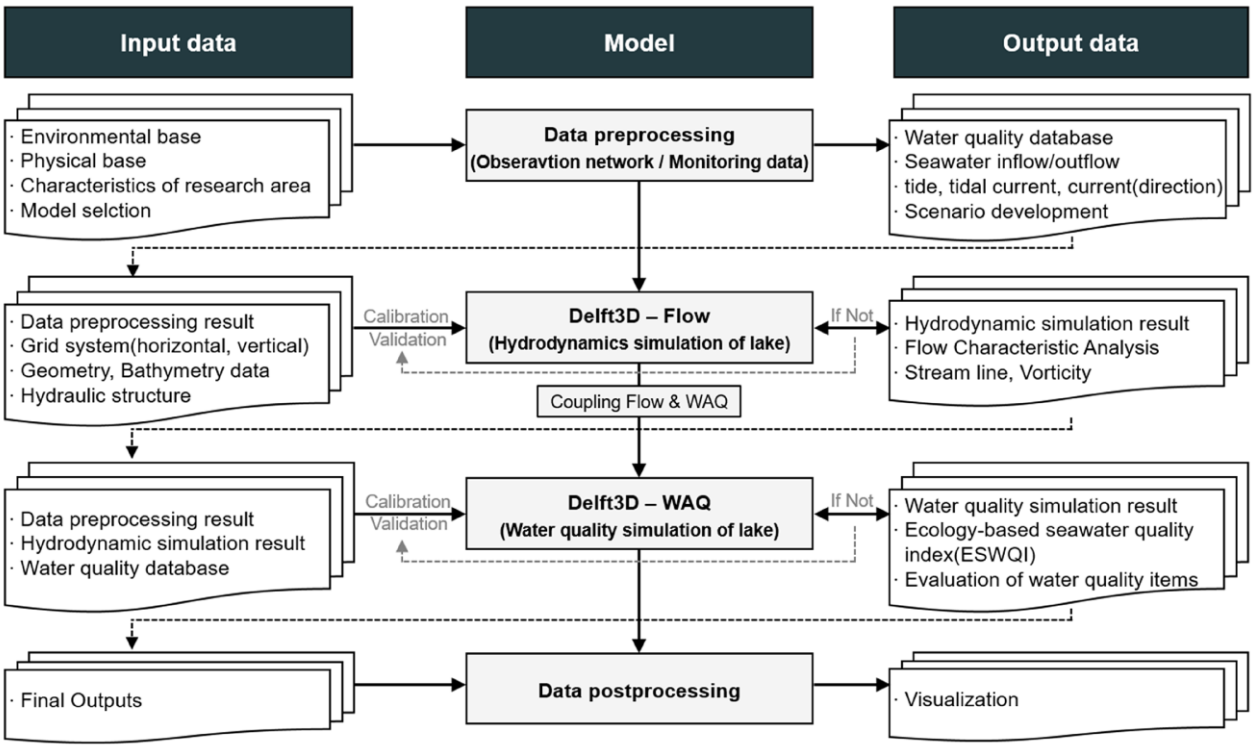

Figure 1. Delft3D modeling and analysis process comprising inputs, model flow, and outputs in each step of the study procedures

2. Material and Methods

2.1. Study Area

Considering the flood control capacity, the managed water level in Saemangeum Lake is maintained at an elevation level (EL) of -1.5 m with inflow and outflow of seawater through Shinsi and Garyuk sluice gates. This strategy prioritizes the inundation effect over lake water quality. When the tide level of the outer sea drops below that of the lake water during ebbing tides, due to decreased outer sea tide levels, both sluice gates are simultaneously opened to drain the water until the lake water level drops to an EL between -1.7 m and -2.0 m. As the tide level outside rises above that of the lake, seawater flows in through the two sluice gates, and the gates close when the lake water level reaches the designated water level [35]. During the neap tide period, when the outer sea tide level is maintained higher than the managed water level of Saemangeum Lake, inflow and outflow of seawater through the sluice gates is not possible. Moreover, the land

use in upstream watershed areas, such as the Mangyeong River basin and Dongjin River basin, predominantly comprises agricultural activities (49.8%) and forestry (34.6%) [36]. Meanwhile, most farmland is located below the watershed areas near Saemangeum Lake. The total phosphorus (TP) load is 3,751 kg/d, with non-point sources accounting for 83% [37]. The target water quality of Saemangeum Lake includes a total organic carbon (TOC) level of 5.0 mg/L and a TP level of 0.05 mg/L [33]. The monitoring stations that represent water quality are ML3 and DL2 (Figure 2).

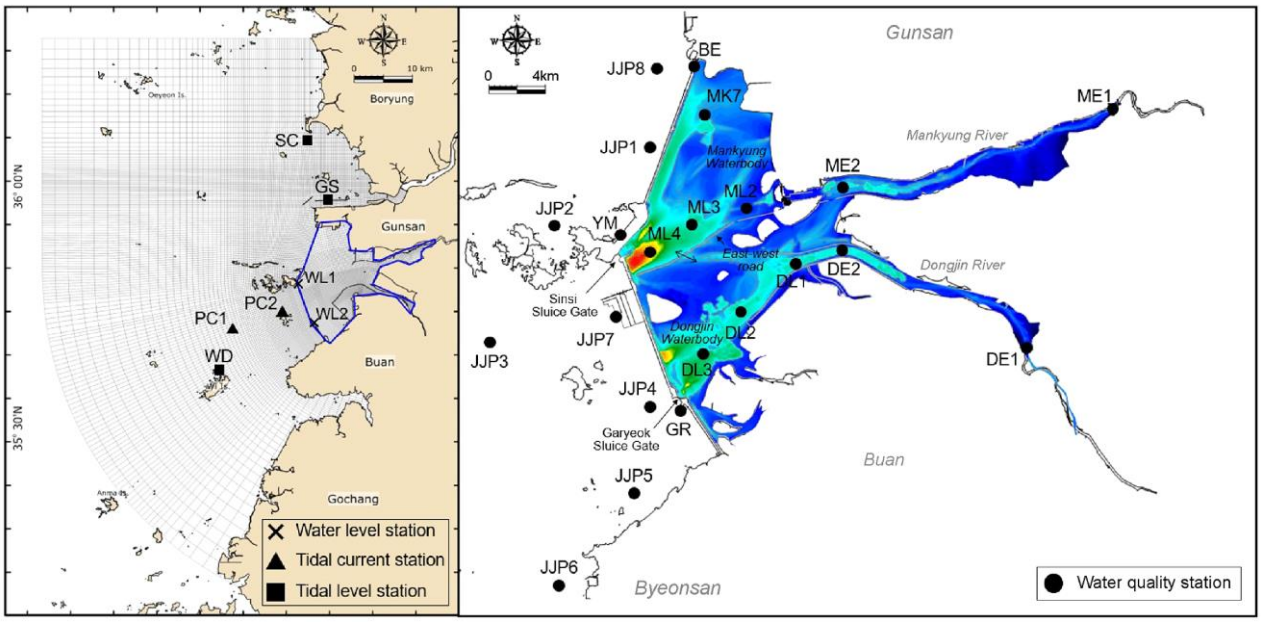

Figure 2. Model grid system and major monitoring stations in Saemangeum Lake

2.2. Data Collection

TOC, TP, chlorophyll-a (Chl-a), total nitrogen (TN), dissolved oxygen (DO), and phosphate phosphorus (PO4-P) data were collected from the Ministry of Environment (MOE) [38], Ministry of Oceans and Fisheries (MOF) [39], and Korea Institute of Marine Science & Technology Promotion (KIMST) [40]. Generally, when evaluating water quality, analysis is performed on Chl-a, TP, TN, and TOC, which have the greatest impact on eutrophication. However, unlike rivers, water quality in lakes is highly dependent on the phytoplankton, while Chl-a is widely used as an alternative indicator of the standing phytoplankton crop [3]. TN and TP serve as nutrients for phytoplankton, causing eutrophication and red tide. Meanwhile, the TOC can reflect the total organic matter relatively accurately through stable oxidation. Hence, TOC was adopted in this study to analyze the amount of organic matter in the lake [35]. Additionally, DO affects various physical and chemical properties of water and can directly affect lake water quality [23]. PO4-P is a component of TP and is the most readily available form of phosphorus utilized by living organisms, including algae [35].

Additionally, sluice gate operation data and inner and outer lake water level data measured by the Korea Rural Community Corporation were collected to estimate the volume of seawater inflow and outflow through the sluice gates. The water quality, water level, and sluice gate operation data covered a 10-year period between 2013 and 2022. Additionally, the tide data, covering January to December 2021, were from the Korea Hydrographic and Oceanographic Agency (KHOA) [41], while the tidal current data included data from winter (February 4 to 19, 2021) and summer (August 19–September 3, 2021). Given that flow velocities inside Saemangeum Lake were not measured, long-term precision monitoring was conducted to acquire high-resolution data. The ML3 station served as the survey site between June 17 and July 27, 2021. The survey items were flow velocities and directions, measured by a 0.5-m vertical interval. A total of 300 data points were collected, with measurements taken at 2 s intervals over 10 min. Subsequently, the average value for each 10-min interval was recorded.

2.3. Calculation of Seawater Inflow

To analyze the relationships between the volume of seawater flowing into Saemangeum Lake and water quality parameters, it was necessary to calculate the seawater volume. However, as the volume of inflow and outflow through the sluice gates was not measured, Equation 1 was applied to estimate the volume:

$$Q = CG \cdot HH \cdot B\sqrt{2g(H_1 - H_2)} \quad (1)$$

where, Q is the flow rate (m^3/s), CG is the flow coefficient, H_1 is the height (m) from the bottom elevation to the upstream water surface, H_2 is the height (m) from the sluice gate bottom elevation to the downstream water surface, HH

is the height (m) from the sluice gate bottom elevation to the bottom of the gate, B is the width (m) of the gate, and g is the gravitational acceleration (m/s^2).

During most of the neap tide season, the low tide has an EL of approximately -0.5 m, with the outer tide level higher than the water level in the lake. Therefore, drainage is difficult for a relatively long time (Figure 3). In contrast, the low tide during the spring tide season has an EL < -3.0 m, facilitating drainage.

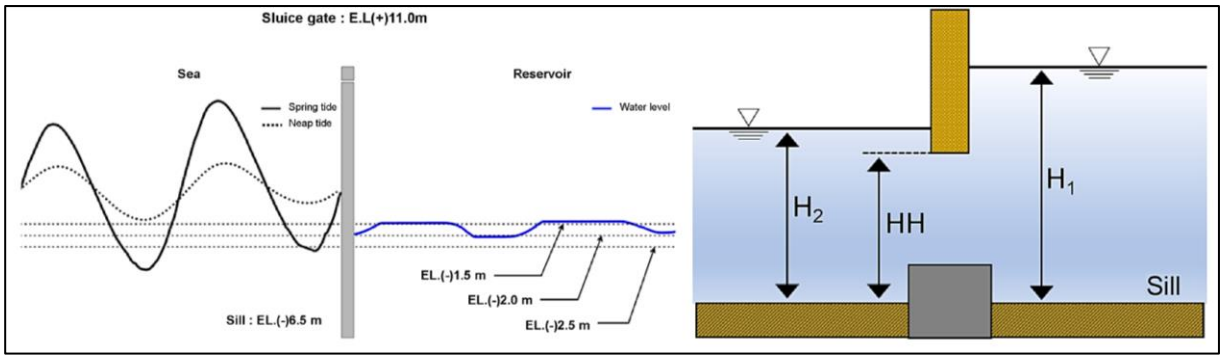

Figure 3. Schematic diagram of seawater circulation through sluice gate and flow rate formula

2.4. Delft3D Model

The Delft3D modeling suite, designed for coastal, river, and estuarine areas, was applied in Saemangeum Lake. It encompasses hydrodynamic, salt and heat transport (Delft3D FLOW), and water quality (Delft3D WAQ) modules. The FLOW module tackles the 3D baroclinic Navier–Stokes and transport equations under the Boussinesq assumption, while the WAQ solves the advection–diffusion–reaction equation for various model substances, drawing hydrodynamic data from the FLOW module [42, 43].

The Saemangeum Lake model area was set as 85 km in the east–west direction and 127 km in the north–south direction, including Yeonggwang to the south and Daecheon to the north relative to portions of Saemangeum in the Yellow Sea. For the horizontal calculation grid network, an orthogonal curvilinear grid system with a minimum of 200 m in the outer sea area in front of the Saemangeum seawall and a minimum of 78 m inside the lake was applied (Figure 2). In the vertical direction, 38 Z-levels were designated perpendicularly. There were 11,272 active grids on the outer side and 5,400 on the inner side of Saemangeum Lake. Grid distortion was maintained below 5°. Meanwhile, Δt, the time interval for numerical calculation, was set to 1 min to satisfy the Courant–Friedrichs–Lewy condition. The simulation period was from January 1 to December 31, 2021; the annual precipitation during 2021 was 1,355.7 mm, corresponding to a normal year (Table S1). The correlation coefficient of the precipitation pattern was 0.87, similar to the average precipitation pattern (Figure S1).

Skill scores (Equations 2 and 3), index of agreement (IOA; Equation 4), and % difference (Equation 5) were applied to quantitatively evaluate the model reproducibility (Table 1). Skill scores were categorized as "excellent" for > 90%, "good" for 80–90%, "average" for 60–80%, and "bad" for < 60% [44]. IOA is a standardized index for the degree of error in predicted values and is used to evaluate the reproducibility of time series data. USEPA considers ≥ 0.5 to indicate good agreement and 1 to indicate a perfect match [45]. With respect to % difference, < 25% for nutrients is considered to indicate "very good" reproducibility [46].

Table 1. Model evaluation index and formula

Index	Item	Equation	
Skill Score	Tidal semi-range, Water quality Major axis size of current	$Skill\ Score = 1 - \left\|\frac{Simulation - Observed}{Observed}\right\|$	(2)
	Phase lag	$Skill\ Score = 1 - \left\|\frac{Simulation - Observed}{360°}\right\|$	(3)
IOA	Water level, Water quality	$IOA = \left[\frac{\left\|\sum_{i=1}^{n}(S_i - O_i)^2\right\|}{\sum_{i=1}^{n}\left(\left\|S_i - \underline{O}\right\| + \left\|O_i - \underline{O}\right\|\right)^2}\right]$	(4)
% difference	Water quality	$\%\ diff. = \frac{\left\|\sum_{i=1}^{n} O_i - \sum_{i=1}^{n} S_i\right\|}{\sum_{i=1}^{n} O_i} \times 100$	(5)

2.5. Streamline and Vorticity

Streamline refers to a curve where the velocity vector at an arbitrary location is parallel to the tangent vector [47], which can be used to easily identify the pattern of flow in a target water body [48]. Assuming steady state and two-dimensional incompressible fluid, streamline can be calculated using Equations 6 and 7 [49]. Steady state can be assumed as streamline was calculated using the seasonal average flow. Vorticity (ω) is an indicator of the degree of rotation of fluid, which can be calculated using Equation 8 [50]:

$$d\Psi = \frac{\partial \Psi}{\partial x}dx + \frac{\partial \Psi}{\partial y}dy \tag{6}$$

$$u = \frac{\partial \Psi}{\partial y}, -v = \frac{\partial \Psi}{\partial x} \tag{7}$$

$$\omega = \frac{\partial v}{\partial x} - \frac{\partial u}{\partial y} \tag{8}$$

where, Ψ is the stream function, x, y represent the coordinates (m) on the orthogonal linear coordinate system, and u, v represent the horizontal flow velocities (m/s) on orthogonal curvilinear coordinate system x, y, respectively.

The geometry and intensity of streamline and vorticity significantly impact the accumulation and retention time of materials [51]. In areas with rotational streamline and intense vorticity, long retention time of water particles and material can lead to an anoxic environment and degradation of water quality [52]. Streamline parameters and vorticity were estimated using the vector average flow of residual current by season, grid, and layer.

2.6. ESWQI

In Korea, the MOF evaluates water quality based on the ESWQI [34], which is a water quality grading standard calculated by evaluating eutrophication-causing items (dissolved inorganic nitrogen [DIN] and dissolved inorganic phosphorus [DIP]), primary reaction items (Chl-a and transparency), and secondary reaction items (DO saturation of the lower layer) [53]. ESWQI is calculated using Equation 9:

$$\begin{aligned} ESWQI = {} & (10 \times [DO\ Saturation\ of\ the\ lower\ layer(DO)]) \\ & + \left(6 \times \left[\frac{Phytoplankton\ concentration(Chla) + Transparency(SD)}{2}\right]\right) \\ & + \left(4 \times \left[\frac{Dissolved\ inorganic\ nitrogen(DIN) + Dissolved\ inorganic\ phosphate(DIP)}{2}\right]\right) \end{aligned} \tag{9}$$

where DO saturation of the lower layer, phytoplankton concentration (Chl-a), transparency (Secchi disk depth [SD]), DIN, and DIP do not reflect absolute concentrations. Instead, they are defined as the scores by water and concentration intervals [54]. The scores for each item by concentration interval in the western central waters, the site of Saemangeum Lake, are shown in Table S2. Calculated ESWQI scores of ≤ 23, 24 – 33, 34 – 46, 47 – 59, and ≥ 60 points were categorized as Grades I, II, III, IV, and V, respectively (Table S3). Transparency (SD) is not calculated in water quality modeling. Accordingly, it was assumed that transparency could be categorized as background extinction, extinction by suspended solids, and extinction by phytoplankton; thus, the relationships among suspended solid concentration, Chl-a concentration, and turbidity were estimated from 2013–2022 using water quality monitoring network data evaluated at the JJP1-8 station.

$$\begin{aligned} Transparency = {} & [-0.38465SS + 0.02167SS^2 - 0.00058SS^3 + 0.00001SS^4] \\ & + [0.38672Chla - 0.09934Chla^2 + 0.00719Chla^3 - 0.00016Chla^4] + 4.19976 \end{aligned} \tag{10}$$

where the term related to SS refers to the influence of suspended solid concentration, the term related to Chl-a refers to the influence of tidal current, and 4.19976 refers to background extinction.

3. Results and Discussion

3.1. Relationship between Target Water Quality and Seawater Inflow

Seawater Inflow Volume and Water Quality Concentration by Year:

The Republic of Korea government has set the following target water quality concentration levels for Saemangeum Lake: TOC (5 mg/L) and TP (0.05 mg/L) [3, 35]. Therefore, the relationship between seawater inflow, TOC, and TP was analyzed. Between 2015 and 2019, when the gates were operated in a diurnal cycle, the average volume of seawater inflow/outflow was approximately 9×10^9 t/year. Between 2019 and 2020, when the gates were operated on a four-diurnal cycle, the average volume of seawater inflow/outflow decreased by 52% to approximately 4.3×10^9 t. In contrast,

in 2013, 2014, 2021, and 2022, when the gates were operated on a semidiurnal cycle for frequent seawater inflow and outflow, the average seawater inflow/outflow volume was approximately 22.9 × 10^9 t/year, representing a 2.6-fold increase compared with that observed when the gates were operated once daily. Thus, the frequency of gate opening and closing directly impacted the volume of seawater inflow/outflow.

TOC and TP concentrations increased during summer when seawater inflow was at a minimum and subsequently decreased to the lowest concentration during winter. The observed increase persisted to the following summer. During summer, seawater inflow was limited due to the need to eliminate a large volume of freshwater inflow from floods. Moreover, the water level inside the lake was maintained at the managed water level. However, due to the rise in water level during flooding, a considerable deviation from the managed water level was not observed. Consequently, the volume of seawater permitted to flow in was low. TOC concentrations generally decreased since 2019 but were high in 2019 and 2020 when seawater inflow was allowed during four-diurnal cycles. In 2013, 2014, 2021, and 2022, when seawater inflow was on a semi-diurnal cycle, the TOC concentration was low, indicating that it was affected by the seawater inflow volume (Figure 4). Although the gate operation frequency affects water quality, as it is directly associated with the seawater inflow volume, the decrease in peak TP concentration only reached 25% even when the seawater inflow volume increased by 8-fold. Additionally, the target water quality criteria were surpassed during summer and winter (Figure 5). Therefore, given the difficulty in achieving visibly improved water quality based only on increasing the seawater inflow volume, non-structural alternatives were required. Accordingly, the relationships between seawater inflow, TOC, and TP concentrations were evaluated, and the seawater inflow volume required to satisfy the target water quality was estimated.

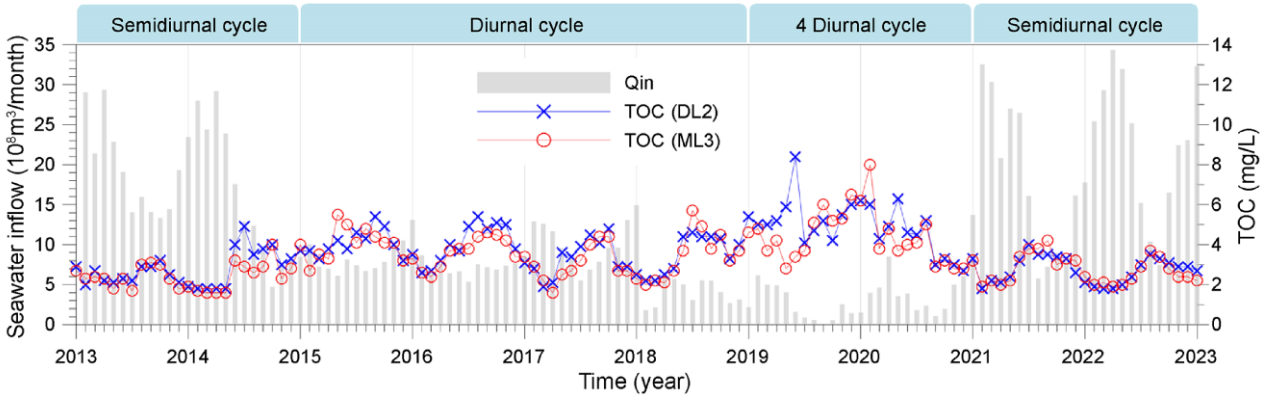

Figure 4. Comparison of seawater inflow and TOC concentration (ML3, DL2)

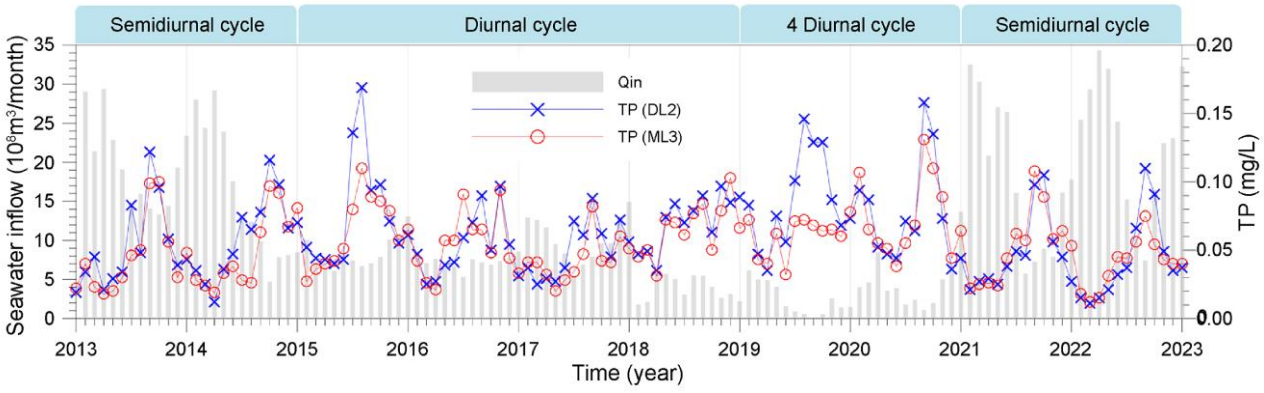

Figure 5. Comparison of seawater inflow and TP concentration (ML3, DL2)

Annual Seawater Inflow and Water Quality Concentration

The relationships between total annual seawater inflow and annual average TOC and TP concentrations were analyzed and the volume of seawater inflow that can meet the target water quality criteria based on annual average water quality was estimated (Figure 6). At the ML3 station, the annual average TOC concentration of 5 mg/L for target water quality was satisfied throughout the analysis period. At the DL2 station, the concentration exceeded only in 2019, when the lowest volume of seawater inflow was recorded at 30 × 10^8 m^3/year. TOC concentration decreased with increasing flow. Particularly, the reduction was noteworthy in the 0–150×10^8 m^3/year interval. However, the reduction effect decreased at ⩾ 150 × 10^8 m^3/year intervals. Hence, the reduction effect on concentration decreased with increasing

flow. Such a relationship was also found with TP concentration. At the ML3 station, the years in which the annual average concentration of 0.05 mg/L, the target water quality, was not satisfied were 2015, 2016, 2018, 2019, and 2020, whereas the target water quality was satisfied in 2013, 2014, and 2022 when semidiurnal cycle was used for seawater inflow. At the DL2 station, the target water quality was not satisfied in all years except in 2021 and 2022, when a semidiurnal cycle was used for seawater inflow. The volume of seawater inflow for satisfying the target water quality was defined as the highest volume of seawater inflow among measured TP concentrations that exceeded the target water quality for conservative evaluation. The results showed that the volume was 217 × 10^8 m^3/year and 237 × 10^8 m^3/year at the ML3 and DL2 stations, respectively.

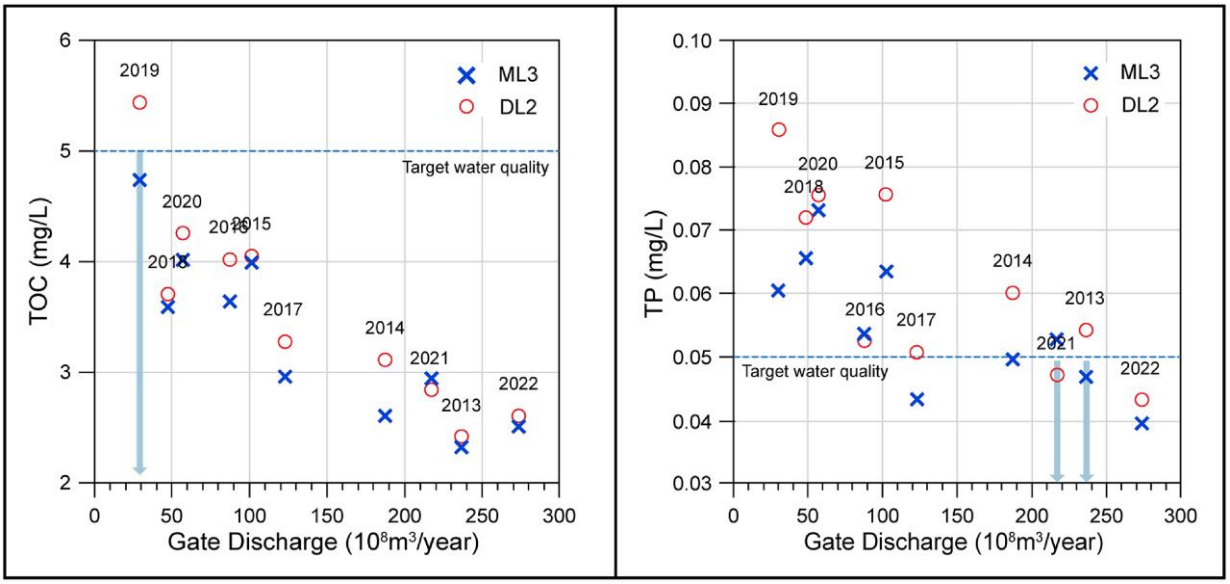

Figure 6. Relationship between annual seawater inflow and average annual TOC

Monthly Seawater Inflow and Water Quality Concentration

At the ML3 and DL2 stations, the monthly average TOC concentration target of 5 mg/L for water quality was predominantly met during the analysis period. The seawater inflow volume estimated to satisfy the target water quality was 7 × 10^8 m^3/month for the ML3 and DL2 stations (Figure 7). For TP, the estimated seawater inflow volume to satisfy the target water quality was 18 × 10^8 m^3/month and 16 × 10^8 m^3/month for the ML3 and DL2 stations, respectively (Figure 8). During summer, when seawater inflow is limited due to flooding, attaining the required level of seawater inflow becomes challenging. Therefore, separate measures are needed to maintain water quality that aligns with the designated targets. Similar to TOC, TP concentration decreased with increasing flow, with a flatter slope of concentration decrease during the ≥ 10 × 10^8 m^3/year intervals with high flow than the 0–10 × 10^8 m^3/year interval with low flow. Hence, the concentration reduction effect decreased with increasing flow.

As seawater inflow increases, the decrease in TP concentration responds less than the decrease in TOC concentration. Phosphate (PO4-P) that flows into the lake is synthesized by the bodies of algae, with a portion of the particulate phosphorus precipitating to the bottom. Moreover, phosphate combined with calcium (Ca) or iron (Fe) is absorbed into the sediment as suspended colloidal particles and becomes re-released into the water layer under anaerobic conditions; the remaining PO4-P is permanently deposited in the bottom sediment [25]. Meanwhile, increased salinity in the water body raises the pH, inhibiting phosphorus absorption onto iron oxide, resulting in limited adsorption in salty marine environments compared to freshwater environments. However, as the ocean is sulfate-rich, Fe(II) in sediments combines with hydrosulfide (HS−). Therefore, if the phosphorus in the porewater combines with iron at relatively low levels, the rate of phosphorus release into the water layer increases [25, 55]. This, in turn, increases the water concentration. Additionally, pollutants may become stagnant or isolated due to slow east–west and vertical flow and limited discharge by sluice gate operation. Therefore, in the case of phosphorus, the effect of reducing its concentration via dilution is relatively poor. Generally, in rivers, when the flow rate increases upstream, water quality improves due to the dilution effect. However, in the case of freshwater lakes, due to the characteristics of stagnant waters with long hydraulic retention times, the flow from upstream does not move downstream and, thus, does not improve water quality. Therefore, seawater flowing in and out through the sluice gate represents the only alternative for improving water quality. However, it is structurally impossible to significantly increase the amount of seawater inflow due to the limited sluice gates. A non-structural alternative would be to change the operation method of the sluice gate to efficiently induce the circulation system of seawater.

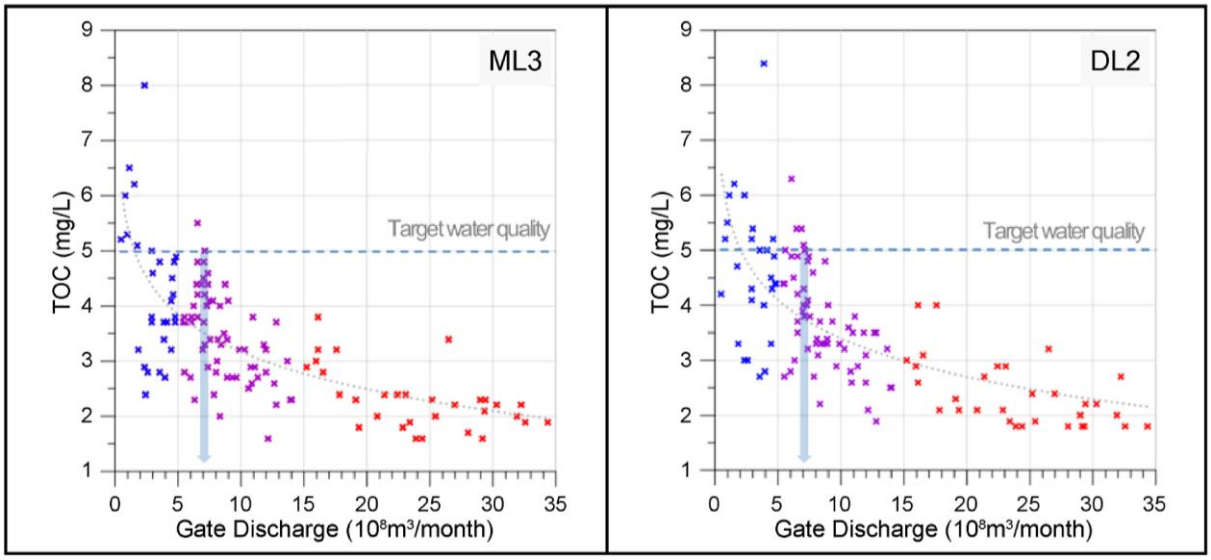

Figure 7. Relationship between monthly seawater inflow and average monthly TOC

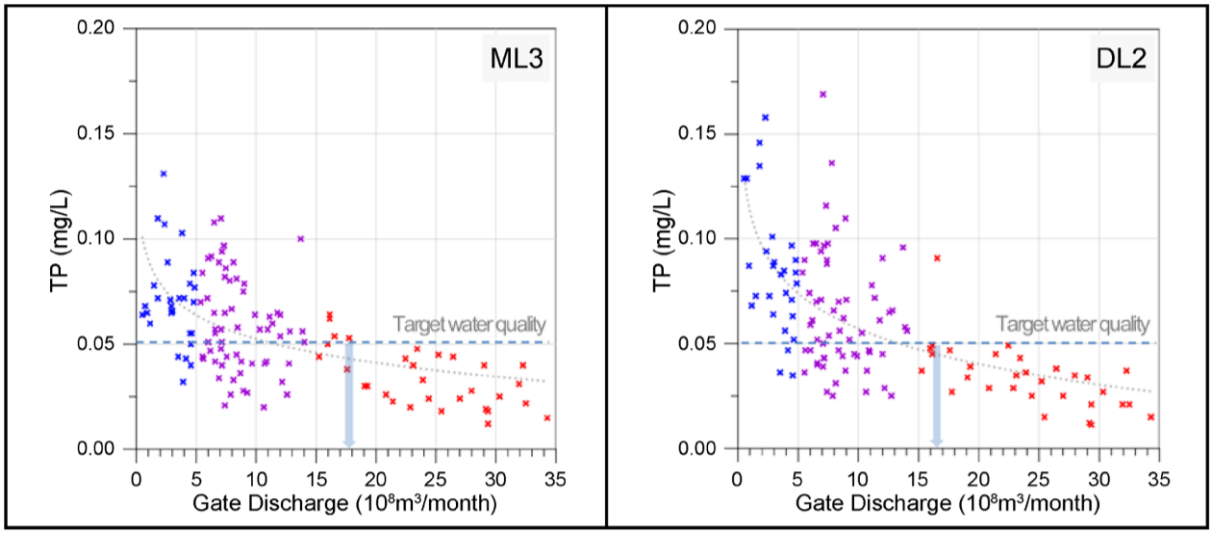

Figure 8. Relationship between monthly seawater inflow and average monthly TP

3.2. Structure of the Scenario

According to the analysis of annual seawater inflow and water quality concentration, the seawater inflow required to meet the target water quality for TP was estimated to be 236.4 × 10^8 m^3/year. Increasing the volume of seawater inflow and maintaining a highly managed water level can be advantageous for improving water quality [56]. Thus, the frequency of seawater inflow was considered, and the water level was managed. Although it is necessary to increase the seawater inflow volume during summer to improve water quality, certain limitations arise during summer due to flood control. Therefore, the alternating operation of sluice gates was applied as a substitute.

For SC-0 and SC-Q1, the frequency of seawater inflow was considered. The frequency of gate opening and closing directly impacts the seawater inflow/outflow volumes. Therefore, the impact according to diurnal and semi-diurnal gate operation was assessed. For SC-R, alternating sluice gate operation (clockwise/anticlockwise) was applied to improve the reverse flow within the lake (Figure 9). Currently, the gate operation involves simultaneously opening and closing both gates to account for the outer and inner water levels during falling and rising tides (Figure 9, left). Such operations repeat movement in the upstream and downstream directions as a two-way current. Consequently, seawater is unable to travel far into the lake and is, thus, incapable of actively diluting the lake water [57]. In contrast, the alternating operation involves staggered opening and closing of the Shinsi and Garyuk sluice gates. With this method, circulation is controlled in a clockwise direction by Shinsi (inflow) → Garyuk (outflow) and in an anticlockwise direction by Garyuk (inflow) → Shinsi (outflow) (Figure 9 Right). The alternating operation involves operating the sluice gates to allow the mixture of flows from clockwise and anticlockwise circulations. That is a clockwise flow is created during the mean and spring tide period and an anticlockwise flow during the subsequent mean and spring period. The alternating cycle was set to 15 days. The gates were operated for clockwise circulation in the lake for 15 days, followed by anticlockwise circulation for 15 days.

For SC-Q2 and SC-Q3, water quality was assessed based on managed water level. A larger difference in the drop in water level from the managed water level implied a greater volume of seawater inflow/outflow. When the water level was reduced by 0.5 m from the managed water level at an EL of -1.5 m to an EL of -2.0 m, the volume of seawater inflow was 107 × 106 m^3 (Table S4). When the managed water level had an EL > -1.3 m and the EL of water was reduced to -2.0 m, the volume of seawater inflow was 152 × 106 m^3 (Table S5), accounting for a 36% increase in available water capacity. When the managed water level was maintained at a lower level, with an EL of -1.7 m, and was reduced to an EL of -2.0 m, the volume of seawater inflow was 64 × 106 m^3 (Table S6), with a decrease in the available water capacity due to a 39% decrease from the managed water level. The simulation conditions for each scenario have been listed in Table 2, and the seawater inflow is shown in Figure 10.

While previous studies have evaluated the dilution effect by increasing the upstream flow rate to improve water quality [16, 21, 23], this study examined increasing seawater inflow and changing the hydraulic circulation system as non-structural alternatives. This scenario was designed with the goal of improving water quality through efficient water management.

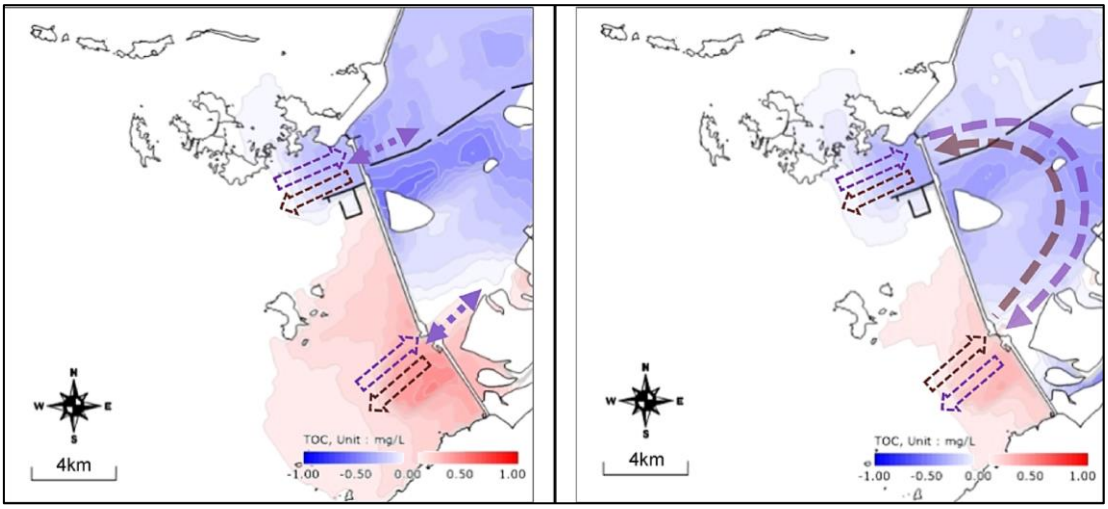

Figure 9. Concept of two-way circulation and one-way alternating circulation flow (Left: Two-way, Right: One-way)

Table 2. Sluice gate operation scenario to improve water quality

Scenario	Management Level(m)	The direction of seawater circulation	Operation cycle	Seawater Inflow (10^9 m^3/year)	Remarks
SC-0	EL -1.5	Two-way	Twice/day	30	Current status (Standard)
SC-Q1	EL -1.5	Two-way	Once/day	15	Change in seawater inflow
SC-R	EL -1.5	One-way	Twice every 2 days	17	Alternating operation: Clockwise–Anticlockwise
SC-Q2	EL -1.7	Two-way	Twice every 2 days	19	Management water level drawdown
SC-Q3	EL -1.3	Two-way	Twice every 2 days	43	Management water level rising

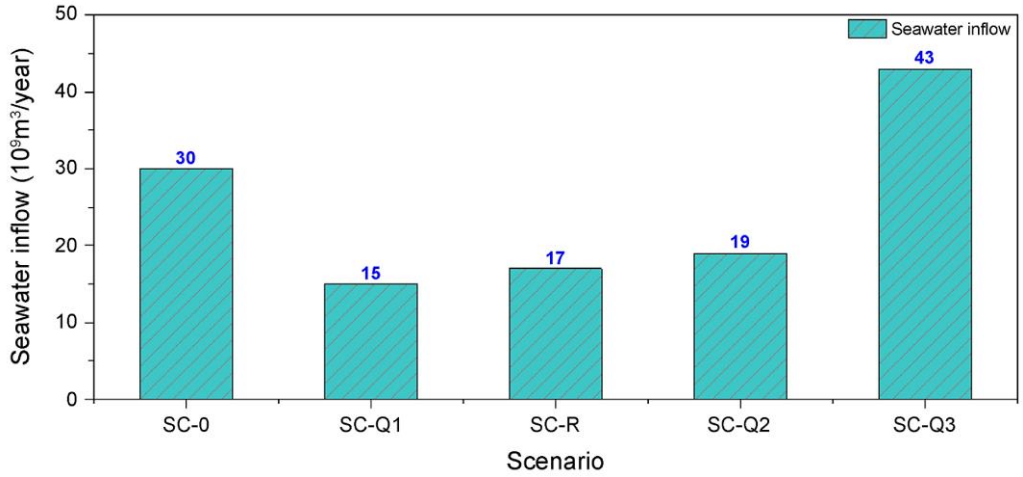

Figure 10. Annual seawater inflow by scenario

3.3. Calibration of Delft3D Model

Tide, Tidal Current, and Water Level

The tides were input to the open boundary at each calculation by synthesizing the five major tidal constituent harmonic constants provided by the "NAO.99jb tidal prediction system" of the National Astronomical Observatory of Japan. Table 3 presents the parameter values used to set up the hydrodynamic model. Major parameters were selected based on the sensitivity analysis results of Koşucu et al. [58]. The model was calibrated by modifying the parameters using the trial and error method.

Table 3. Parameters applied in the hydrodynamic model

Parameter	Unit	Manual	Calibration Value	Reference
Manning Roughness Coefficient	$s/m^{1/3}$	0.02	0.02	
Horizontal Eddy Viscosity	(m^2/s)	1	1.5	
Slope in log–log spectrum	-	-1.6667	-1.6667	[58]
Prandtl–Schmidt Number	-	0.7	0.7	
Spatial Low-Pass Filter Coefficient	-	0.3	0.295	

For five major tide components M_2, S_2, K_1, O_1, and N_2, the average recall of semi-range and phase-lag were 99.4% and 99.0%, respectively. For these five major tidal current components the recall of tidal current velocity (major axis size) was 51.2–99.5%, and the total average was 85.8%. Based on the flow model recall evaluation criteria, the recall was "excellent" for tide and "good" for tidal current. Among tidal harmonic constants, the diurnal tide components K_1 and O_1 had a small size ($\leq$ 0.1 m/s). Consequently, the recall was calculated to be relatively small. However, the effect on the overall tidal current velocity was small, and the total average recall was evaluated as "good" (85.8%; Table 4).

Table 4. Model's tide and tidal current recall (Skill score)

Component tide		Tide (%)		Tidal current (%)
		Semi-range	Phase-lag	Major axis size
Average by measurement station	M_2	99.9	98.9	99.5
	S_2	98.8	99.3	80.3
	K_1	99.7	99.7	59.1
	O_1	95.8	99.2	51.2
	N_2	99.9	94.4	92.6
Total average		99.4	99	85.8

In the time series comparison of tides and tidal currents, the results showed that fluctuation characteristics, such as diurnal inequality and spring-neap fluctuation of tides and tidal currents were reproduced (Figures 11 and 12). At the PC2 station, the phase lag of the tidal current appeared faster than the measured value. This was potentially attributed to the spatially complex flow characteristics due to Saemangeum's new port breakwater and shore protection construction near the PC2 station.

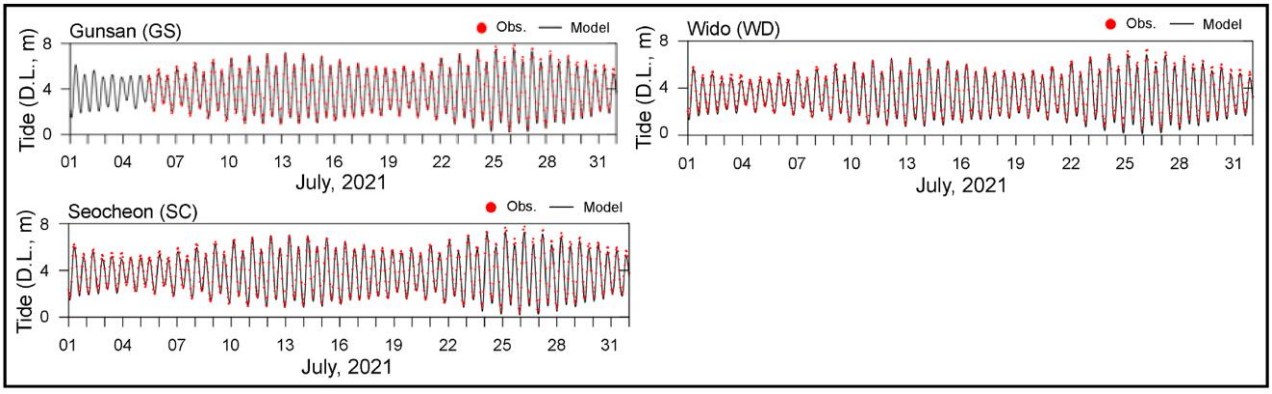

Figure 11. Tidal level time series calibration results (GS, WD, SC)

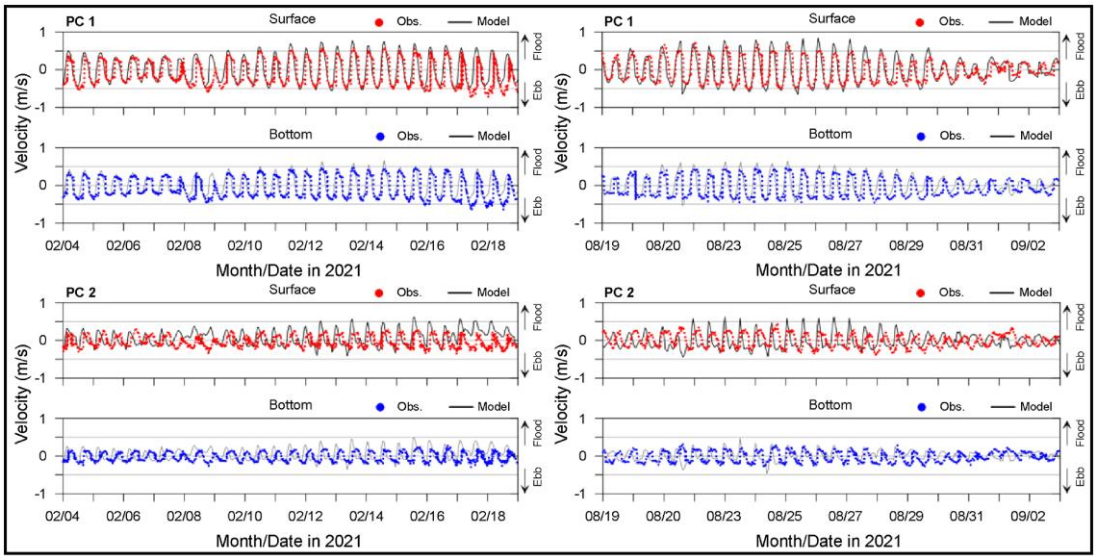

Figure 12. Tidal current time series calibration results (PC1, PC2)

In the time series comparison of the WL1 station within Saemangeum Lake, the IOA was 0.94, indicating "good agreement" with the USEPA criteria. This suggests that the rise in water level inside the lake during inflow and outflow through the gates was accurately reproduced (Figure 13). In particular, the rise in water level during the neap tide period when the gates were not in operation was also reproduced. Hence, river inflow from upstream was properly designated. The calibration results show that the model reproduced the tide propagation, tidal current characteristics, and Saemangeum Lake water level fluctuation characteristics of the study area.

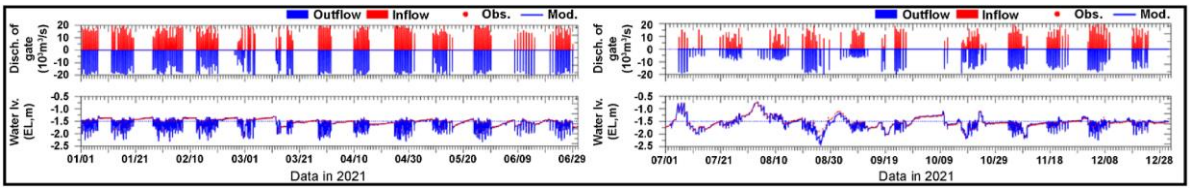

Figure 13. Water level time series calibration results

Among the flow velocity data recorded at the ML3 station, surface, mid, and bottom layer data were extracted and compared to the modeling results (Figure 14). Surface, mid, and bottom layers were defined as upper 20%, 50%, and bottom 80%, respectively. A low-pass filter with a 4-h cutoff cycle was applied to the data for each layer to remove short-cycle components, leaving only the long-cycle components for comparison. The measured values and modeling results were not quantitatively compared as the flow velocity was very slow ($\leq$ 3 cm/s). Rather, time series fluctuation characteristics and two-way circulation recall were qualitatively compared. However, due to a low flow velocity of < 5 cm/s and irregular fluctuation, reproducibility was lower than that of tidal currents with relatively higher flow velocity and iterative flow characteristics. Nevertheless, the overall characteristics were similar to the measured values.

The flow velocity and temporal change characteristics for each layer were reproduced, whereas the characteristics with repeating upstream (+) and downstream (-) flow appeared similarly. In particular, two-layer circulation with downstream flow in the surface layer and upstream flow in the mid or bottom layers was reproduced, indicating that long-term circulation and distribution of materials could be reproduced.

Previous studies targeting lakes have primarily verified water levels only when assessing hydraulic properties [16–26]. Meanwhile, no data have been reported on the flow velocity and direction of Saemangeum Lake, with no verification cases [23–26]. Therefore, the flow velocity, direction monitoring, and model verification conducted in this study are positive achievements.

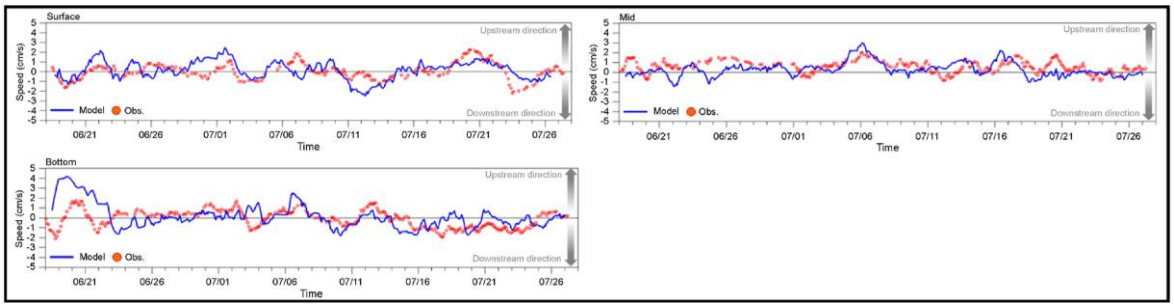

Figure 14. Flow velocity time series calibration results obtained at the ML3 station using precise measurement data

Water Quality

Many coefficients were input into the water quality model, including the growth rate, mortality rate, and feeding rate of phytoplankton, the sedimentation rate, carbon: Chl-a ratio, nitrogen: carbon ratio in algae, and extinction coefficient. The model was calibrated through trial and error, with the major parameters presented in Tables 5–6. In water bodies, physicochemical reactions vary in time and space. Moreover, models may have uncertainties as they are reproduced in rough formulas and parameters. Hence, sensitivity analyses must be performed to clearly identify the influence of parameter values on model results, something rarely reported for Delft3D-WAQ model parameters. The sensitivity analysis for the Delft3D model in the current study primarily comprised the physical parameters of the hydrodynamic model. However, in the case of water quality models, parameters exist for each water quality item and closely interact with each other. Thus, more in-depth analysis considering the dynamic response of water quality model parameters is warranted.

Table 5. Parameters applied in the water quality model

Parameter	Description	Unit	Calibration value
SWSatOxy	Switch saturation DO calculation	-	2.000
ThrAlgNH4	Threshold concentration uptake ammonium	gN/m^3	0.000
ThrAlgNO3	Threshold concentration uptake nitrate	gN/m^3	0.000
ThrAlgPO4	Threshold concentration uptake phosphate	gP/m^3	0.000
RcDen20	MM-denitrification reaction rate at 20 ºC	$gN/m^3/day$	0.100
TcDenWat	Temperature coefficient for denitrification	-	1.070
KsNiDen	Half saturation constant for nitrate consumption	gN/m^3	0.500
KsOxDen	Half saturation constant for oxygen inhibition.	g/m^3	1.000
CTDEN	Critical temperature for denitrification	ºC	2.000
KsAmNit	Half saturation constant for ammonium consumption	gN/m^3	0.500
KsOxNit	Half saturation constant for DO cons.	g/m^3	1.000
CTNit	Critical temperature for nitrification	℃	3.000
COXNIT	Critical oxygen concentration for nitrification	g/m^3	1.000
RcNit	First-order nitrification rate	1/day	0.100
OOXNIT	Optimum oxygen concentration for nitrification	gO_2/m^3	5.000
CFLNIT	Oxygen function level for oxygen below COXNIT	-	0.000
SWRear	Switch for oxygen reaeration formulation (1–13)	-	1.000
TCRear	Temperature coefficient for reaeration	-	1.016

Table 6. Parameters applied in the water quality (algae) model

Parameter	Description	Unit	Calibration Value	Ref. range	Reference
PPMaxFDI (E,P)	Pot. maximum growth rate at 0 dg C FDIATOMS	1/day	0.35	0.07–9.20	Cole and Wells (2003) [59]
PPMaxBLU (E,N,P)	Pot. maximum growth rate at 0 dg C BLUEGRN		0.048–0.056		
PPMaxGRE (E,N,P)	Pot. maximum growth rate at 0 dg C GREENS		0.068		
PPMaxMDI (E,N,P)	Pot. maximum growth rate at 0 dg C MDIATOMS		0.066–0.083		
PPMaxDIN (E,N,P)	Pot. maximum growth rate at 0 dg C DINOFLAG		0.112–0.132		
ChlaCFDI (E,P)	Chlorophyll-a:C ratio per algae type FDIATOMS	gChla/ gC	0.025–0.040	0.01–0.50	EPA (1985) [60]
ChlaCBLU (E,N,P)	Chlorophyll-a:C ratio per algae type BLUEGRN		0.020–0.033		
ChlaCGRE (E,N,P)	Chlorophyll-a:C ratio per algae type GREENS		0.025–0.033		
ChlaCMDI (E,N,P)	Chlorophyll-a:C ratio per algae type MDIATOMS		0.010–0.053		
ChlaCDIN (E,N,P)	Chlorophyll-a:C ratio per algae type DINOFLAG		0.007–0.029		
NCRFDI (E,P)	N:C ratio per algae type FDIATOMS	gN/ gC	0.188–0.210	0.05–0.43	EPA (1985) [61]
NCRBLU (E,N,P)	N:C ratio per algae type BLUEGRN		0.125–0.225		
NCRGRE (E,N,P)	N:C ratio per algae type GREENS		0.175–0.275		
NCRMDI (E,N,P)	N:C ratio per algae type MDIATOMS		0.070–0.255		
NCRDIN (E,N,P)	N:C ratio per algae type DINOFLAG		0.064–0.163		
VsedFDI (E,P)	Sedimentation velocity algae FDIATOMS	m/day	0.02	0.01–0.03	Bowie et al (1985) [61] Shimoda & Arhonditsis (2016) [62] Maggio et al. (2016) [63]
VsedBLU (E,N,P)	Sedimentation velocity algae BLUEGRN		0.02		
VsedGRE (E,N,P)	Sedimentation velocity algae GREENS		0.02		
VsedMDI (E,N,P)	Sedimentation velocity algae MDIATOMS		0.02		
VsedDIN (E,N,P)	Sedimentation velocity algae DINOFLAG		0.02		
ExtVlIM1	VL specific extinction coefficient IM1	m^2/ gDM	0.1	0.05–0.10	Pennock (1985) [64]
ExtVlIM2	VL specific extinction coefficient IM2		0.1		
ExtVlIM3	VL specific extinction coefficient IM3		0.1		
ExtVlBak	Background extinction visible light	1/m	0.11	0.038–0.110	Pennock (1985) [64]

One-to-one comparisons were made with the observed and simulated values for major water quality items. Furthermore, a time series comparison was performed for each station, and recall was calculated. One-to-one comparison results showed that DO was scattered slightly more than other items, which could be attributed to the characteristically large spatiotemporal fluctuation of DO (Figure 15).

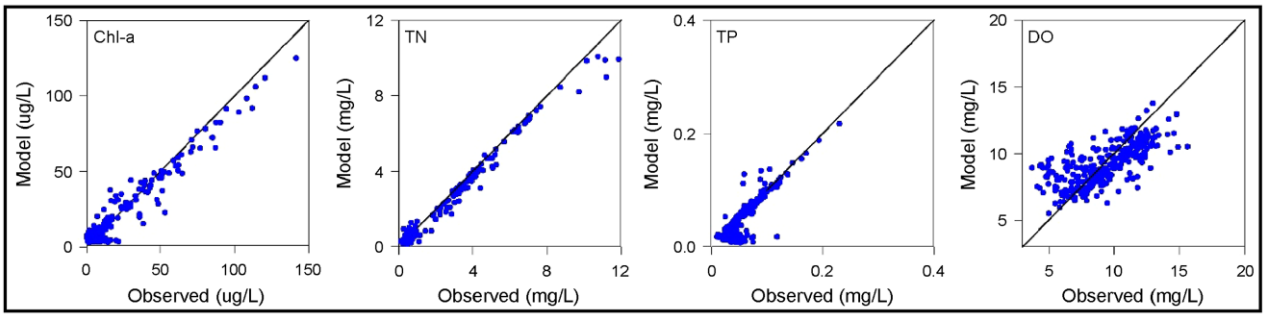

Figure 15. One-to-one comparison of water quality observations and model results

With the water quality calibration stations divided into river, dike inner, dike outer, and KIMST (Table 7), the recall rate of major water quality items were calculated (Table 8). The skill scores for Chl-a, TN, TP, DO, and TOC were 81.6%, 83.9%, 75.1%, 93.2%, and 76.9%, respectively. The IOA of Chl-a, TN, TP, DO, and TOC showed recall rates of 0.69, 0.68, 0.89, 0.76, and 0.68, respectively. Meanwhile, the percentage difference for all items was < 25%, corresponding to "very good." A high percentage difference in TP was observed in sections of the outer Saemangeum Lake as the concentration in this area was low (0.02–0.04 mg/L), and the absolute error was small (< 0.01 mg/L).

Table 7. Classification of water quality model calibration stations

Category	Station	Measurement period	Measuring Institution
River	ME1, DE1	Four times/month	MOE
Dike Inner	ME2, ML1-ML4 DE2, DL1-DL4	Once/month	
Dike Outer	JJP1-JJP8	Four times/year	MOF
KIMST	BE, YM, GR	Once/week	KIMST

Table 8. Recall rate for each major water quality item of the model

Index	Category	Chl-*a*	TN	TP	DO	TOC	Average
Skill score	River	95.8	91.9	99.1	89.7	79.6	91.2
	Dike Inner	76	79.9	94.4	95.6	88.5	86.9
	Dike Outer	71.7	90.9	49.9	95.8	-	77.1
	KIMST	82.7	72.9	56.9	91.6	76.9	76.2
	Total	81.6	83.9	75.1	93.2	81.7	83.1
% diff.	River	4.3	7.8	0.5	11.4	25.6	9.9
	Dike Inner	6.7	17	5.2	3.4	10.3	8.5
	Dike Outer	24.8	5.8	45.6	5.3	-	20.4
	KIMST	9.9	23.6	36.8	5.9	18.8	19
	Total	11.4	13.5	22	6.5	18.2	14.3
IOA	River	0.98	0.99	0.99	0.86	0.73	0.91
	Dike Inner	0.77	0.65	0.85	0.83	0.74	0.77
	Dike Outer	0.8	0.74	0.88	0.63	-	0.76
	KIMST	0.22	0.32	0.83	0.71	0.58	0.53
	Total	0.69	0.68	0.89	0.76	0.68	0.74

In the time series comparison for the ML3 and DL2 stations, the results showed that the model had accurately reproduced the measured values (Figures 16 and 17), especially the TP concentration that increased by non-point input after flooding in August. In the JJP4 and JJP7 stations located in waters in front of the Shinsi and Garyuk sluice gates, the short-cycle concentration change was relatively large, with a transient increase in concentration observed (Figs. S2 and S3). Such findings indicate that effluent discharge from the gates influenced the increased concentrations in the

stations and that such change tended to be large especially after rainfall due to the significant influences of freshwater. While the model relatively accurately reproduced the annual fluctuation characteristics of Chl-a, the model values were slightly overestimated compared with the measured values in mid-July. This can be attributed to the fact that in nature, tidal currents show rapid changes due to adaptation to the water environment, interspecific competition, and feeding, whereas a model may be limited in accounting for all of these factors. Although the model slightly overestimated Chl-a concentrations in the outer part of Saemangeum Lake, the overall annual fluctuation characteristics of the measured values were closely reproduced, indicating that the influence of seawater inflow was adequately accounted for (Figures. S4–S21).

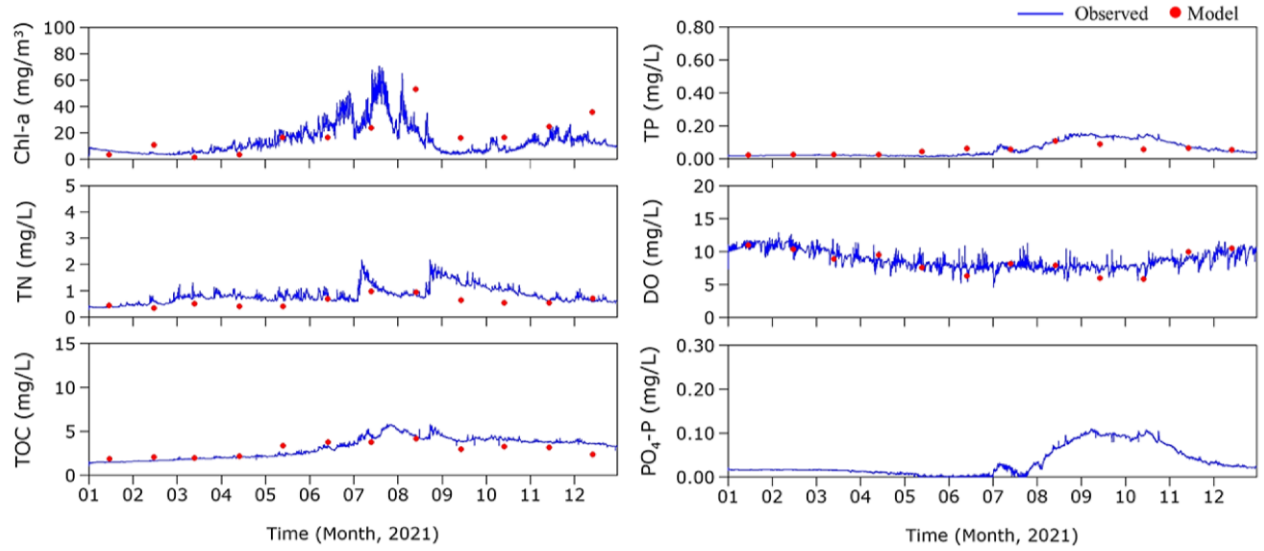

Figure 16. Water quality time series calibration results (ML3)

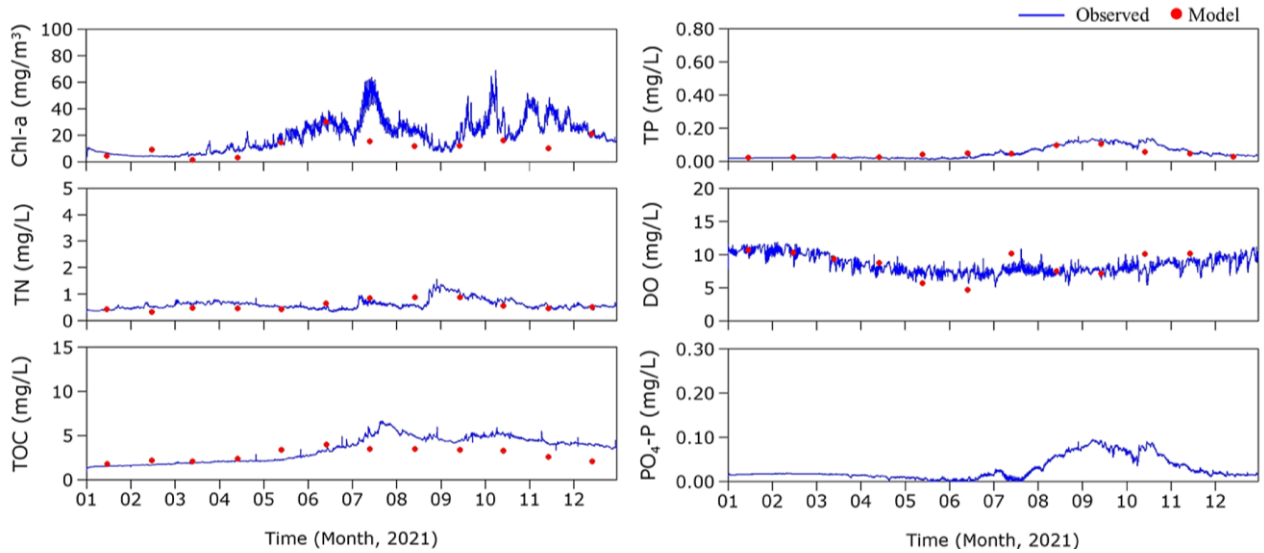

Figure 17. Water quality time series calibration results (DL2)

3.4. Flow Distribution Simulation Results

Analysis of Velocity Distribution and Low Velocity Section

The seasonal and water layer-specific velocity distribution was calculated (Figure 18). In spring, a downstream flow occurs in the surface layer, and an upstream flow is formed in the lower layer, resulting in a two-layer circulation. In the northern portion of the Mangyeong waterbody, clockwise eddies are formed in the surface and bottom layers. The surface and bottom layers are dominated by northward and southward flow, respectively. In summer, the pattern is similar to that of spring, but the surface flow velocity is stronger. However, the area where the two-layer circulation flow appears is expanded further in the summer. In the lower layer, the upstream flow along the east–west two-axis road appears all the way to the lower reaches of the Mangyeong River and Dongjin River. Additionally, a southward flow opposite to the surface is observed in front of the No. 4 dike. The autumn flow pattern was similar to that of spring, but the surface current velocity was stronger, and the upstream flow was stronger in the lower reaches of the Dongjin River. Meanwhile, the current velocity throughout the lake increased in winter. This may be due to the increased seawater inflow and strong northwest monsoon in winter.

Saemangeum Lake has a sufficient wind drift distance exceeding 10 km in the No. 4 dike section, which is sufficient for a wind-driven current to form. In contrast, the eddies that occur in the northern section of the Mangyeong River appear narrow and weak in the central section, unlike in other seasons. The southward-facing eddy current merges with the flow of the Mangyeong River channel so that its residence time does not increase significantly. In the estuary reservoirs where freshwater flows, the baroclinic force acts from the open sea toward the coast in the bottom layer due to the horizontal salinity gradient; meanwhile, the barotropic force acts from the coastal river toward the open sea at the surface layer. In this way, a two-layer circulation structure is formed (Figures 14 and 18). This circulation and mixing of seawater are caused by the density difference created by the interaction between freshwater and seawater.

In general, the effect of salinity is greater than that of water temperature. Indeed, the two-layer circulation structure influences biological, chemical, and sedimentary processes. The eddies occurring in front of the No. 4 dike are likely caused by the wind-driven current along the dike and by the deep water and topography. In all seasons, a two-layer circulation is formed and eddies are maintained in the northern section of the Mangyeong waterbody, which increases the residence time, creating conditions that are vulnerable to water quality management. Thus, to properly manage water quality, it is necessary to reduce the residence time by suppressing the two-layer circulation caused by the horizontal gradient of eddy strength and density.

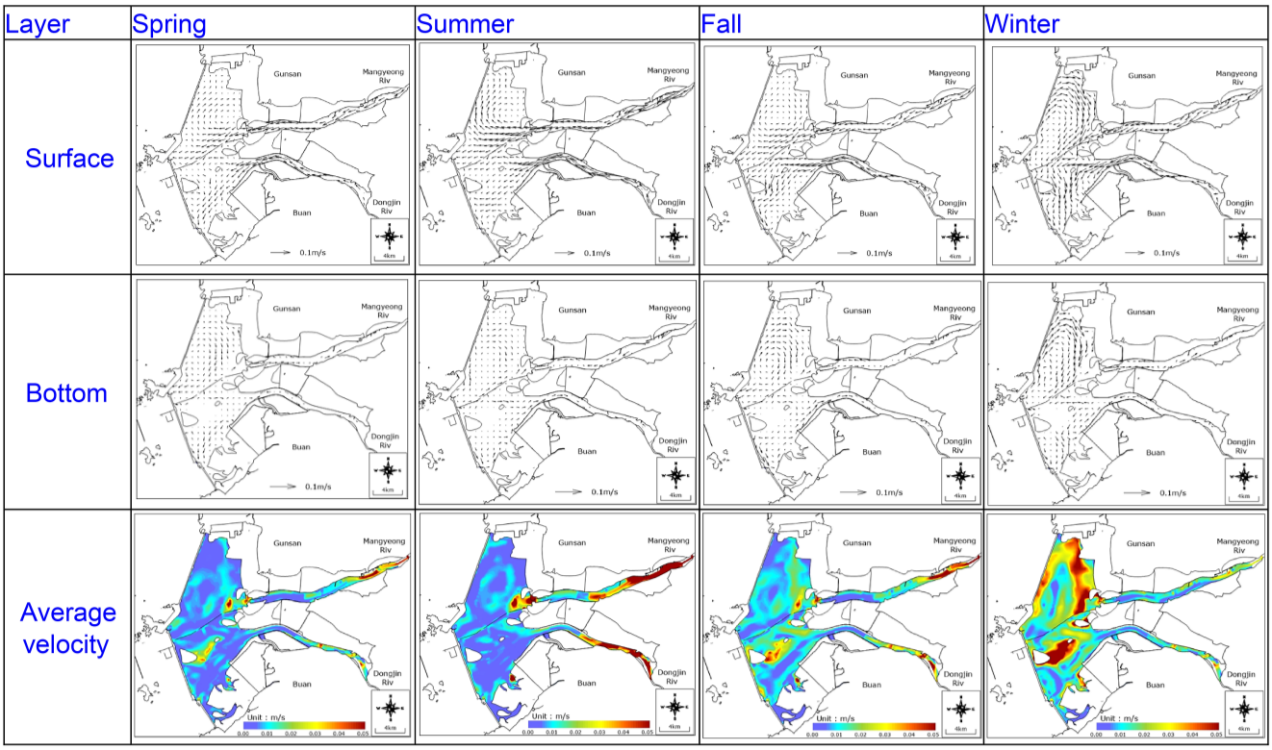

Figure 18. Seasonal velocity vectors and average velocity distributions at the surface and bottom layers

Evaluation of Streamline and Vorticity by Scenarios

In SC-0 with semidiurnal gate operation, downstream flow toward the gates was observed in the intervals that connect the Shinsi sluice gate with the Mangyeong River and the Garyuk sluice gate with the Dongjin River. In the northern part of the Mangyeong area (MK7–ML3 section), a clockwise vortex is formed. In the northern part of the Mangyeong area (MK7–ML3 section), the downstream section of Mangyeong River, and some downstream sections of Dongjin River, upstream flow is created in the bottom layer, which is in the opposite direction to the flow on the surface layer. Consequently, two-layer circulation occurs (Figure 19). In the SC-Q1 scenario with reduced seawater inflow from diurnal gate operation, no significant difference was observed compared with SC-0; however, weaker flow occurred due to wider streamline gap (Figure 20). That is, as the amount of seawater inflow decreases, the flow between the surface and bottom layers becomes separated by density stratification, and the flow is limited in the bottom layer. Hence, the actual retention time can increase at low layers [65].

In the SC-R scenario with alternating one-way circulation in 15-day cycles, the flow in the surface layer was generally similar, while the flow near the southern region of the east–west road was slightly stronger. In the bottom layer, a clockwise vortex was formed on the surface in the northern portion of the Mangyeong waterbody (MK7–ML3 section), unlike SC-0. Moreover, the flow was stronger in the bottom layer in the interval that crossed the east–west road and connected Mangyeong and Dongjin areas (Figure 21). As the flow strengthens and clockwise eddies occur on the surface north of the Mangyeong waterbody area (MK7–ML3 section), the challenge of long-term pollutant retention is expected to be alleviated.

In SC-0, the flow in the surface and bottom layers appeared in the same direction only in certain sections; however, the flow was weak or exhibited no particular trend in most areas. In the SC-Q2 scenario with a decreased managed water level and the SC-Q3 scenario with an increased managed water level, the streamline intensity of vorticity and geometry exhibited some differences; however, overall, the flow characteristics were similar to those in the SC-0 scenario. The SC-Q3 scenario, with greater seawater inflow/outflow from elevated managed water levels, exhibited faster flow due to a narrower streamline gap compared to the SC-2 scenario with less seawater inflow/outflow (Figures 22 and 23). As the amount of seawater inflow increased, the retention time in the lake decreased, and the stagnant water area was reduced. Thus, the increased water level is predicted to exert an overall impact on the lake.

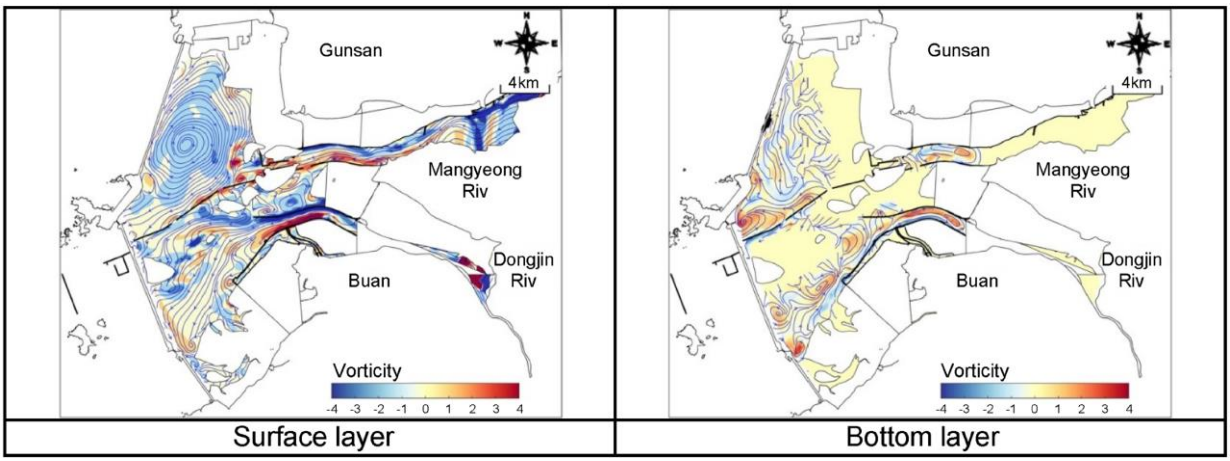

Figure 19. Annual average streamline and vorticity distribution (SC-0)

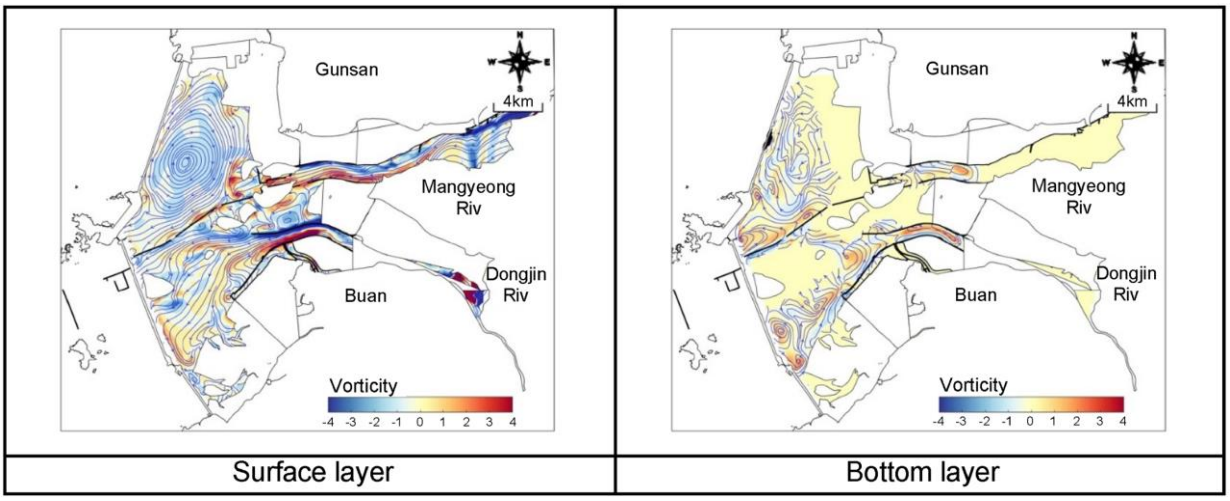

Figure 20. Annual average streamline and vorticity distribution (SC-Q1)

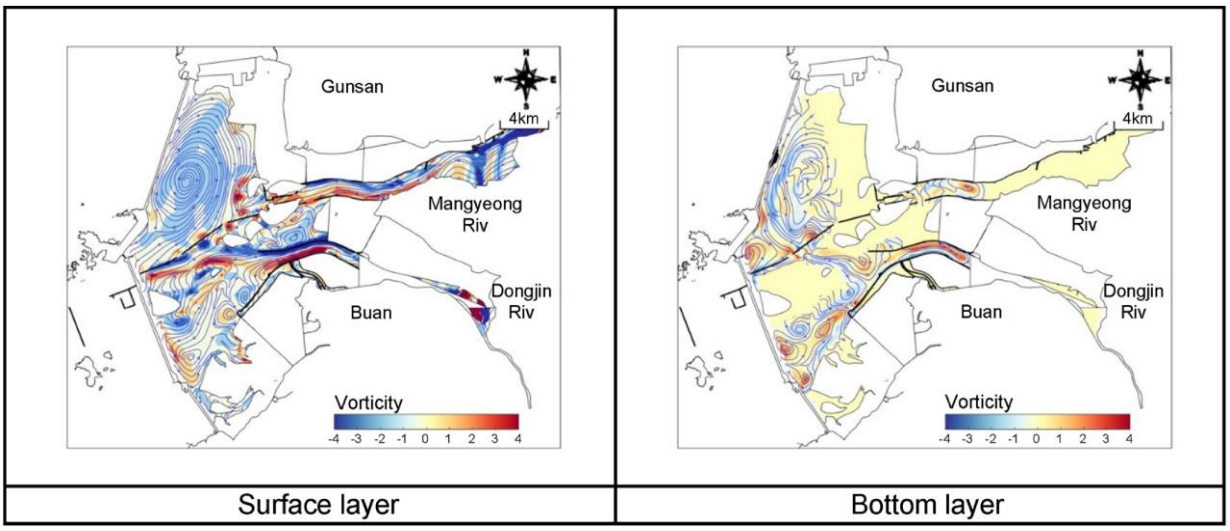

Figure 21. Annual average streamline and vorticity distribution (SC-R)

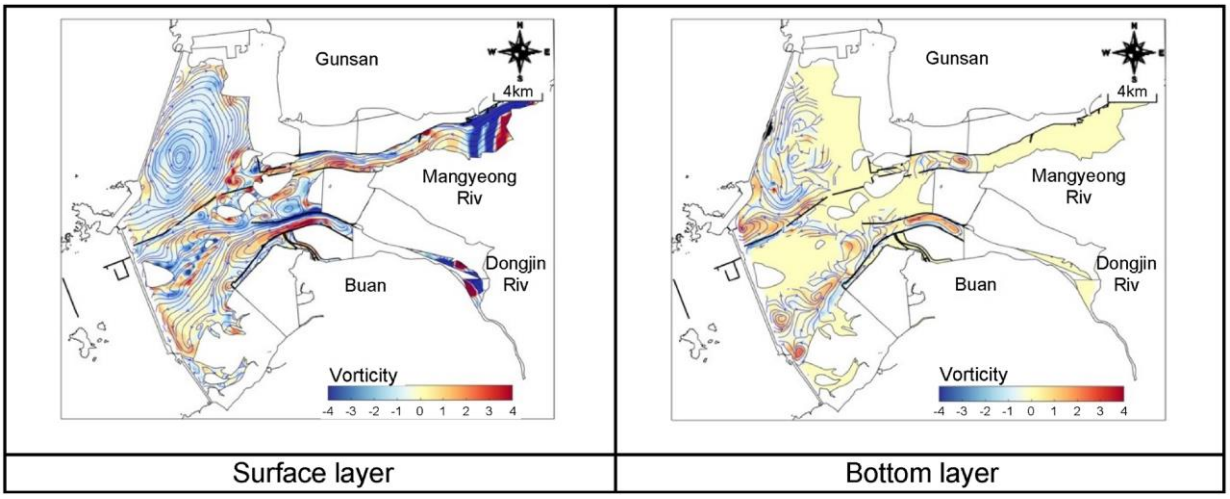

Figure 22. Annual average streamline and vorticity distribution (SC-Q2)

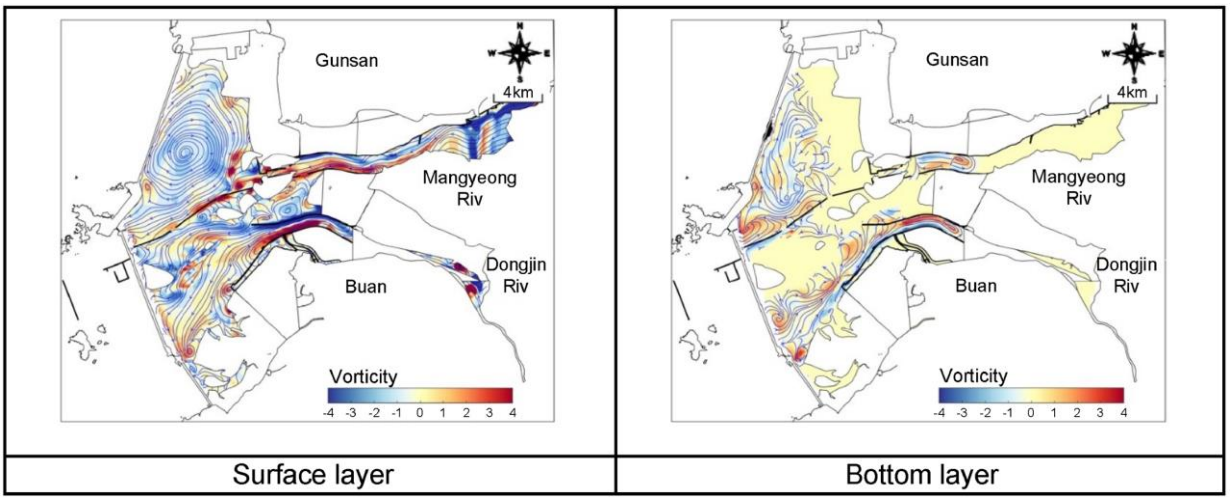

Figure 23. Annual average streamline and vorticity distribution (SC-Q3)

Evaluation of ESWQI

In the SC-0 scenario, the ESWQI in most areas within the lake was ~Grade V during the spring, summer, and fall. During the winter, the ESWQI corresponded to Grade V in Mangyeong River and Dongjin River, approximately Grade III near Shinsi and Garyuk sluice gates, and approximately Grade IV in the other areas (Figure 24). In the SC-Q1 scenario, the ESWQI increased to Grade III–IV in areas near Shinsi and Garyuk sluice gates, which had an ESWQI of Grade III during the winter (Figure 25). In the SC-R scenario, the Grade V ESWQI near the Shinsi and Garyuk sluice gates during spring was improved to approximately Grade IV, and an ESWQI of Grade IV was noted throughout Dongjin area. Areas with an ESWQI of Grade IV were also found near the gates during the fall. During the winter, an ESWQI of ~Grade III was noted throughout the lake, indicating an improvement from the values recorded during the SC-0 (Figure 26). In the SC-Q2 scenario, the Grade IV ESWQI near the Shinsi and Garyuk sluice gates during spring disappeared almost completely (Figure 27). In the SC-Q3 scenario, an improved ESWQI around the gates was observed during spring, fall, and winter. Notably, the ESWQI improved to approximately Grade III during the winter season in most areas around the lake, excluding Mangyeong River and Dongjin River (Figure 28).

At the ML3 and DL2 stations that represent water quality, pie graphs were generated to compare the contribution of each of the five items for ESWQI calculation, and the items with the largest influence on ESWQI were identified (Figure 29). In the SC-0 station, Chl-a concentration had the most remarkable influence on ESWQI grade in most stations and seasons. The DO saturation of the lower layer also had a significant influence. In the midstream/downstream section, the DO saturation of the lower layer had a larger influence on the Mangyeong area with relatively deeper waters. Transparency, which exhibits large spatiotemporal fluctuations, tended to exhibit large seasonal variability. Meanwhile, DIP concentration was an important factor during the summer and fall due to the persistent influence of phosphorus input from non-point sources introduced during flooding in summer [66]. In the SC-Q1 scenario, the influence of DIN was higher than in the SC-0 scenario at the ML3 and DL2 stations, whereas the influence of DIP also increased during the fall. The contribution from transparency decreased slightly in all seasons except spring. In the SC-R scenario, the influence of DIN decreased; it also decreased during the fall. Additionally, the influence of transparency decreased during the fall and winter. The results for the SC-Q2 scenario were similar to those in the SC-0 scenario, with a slightly diminished influence of transparency during the summer. In the SC-3 scenario, the influences of Chl-a and DIN during spring and the influence of DIN, DIP, and transparency during fall were lower than in the SC-0 scenario.

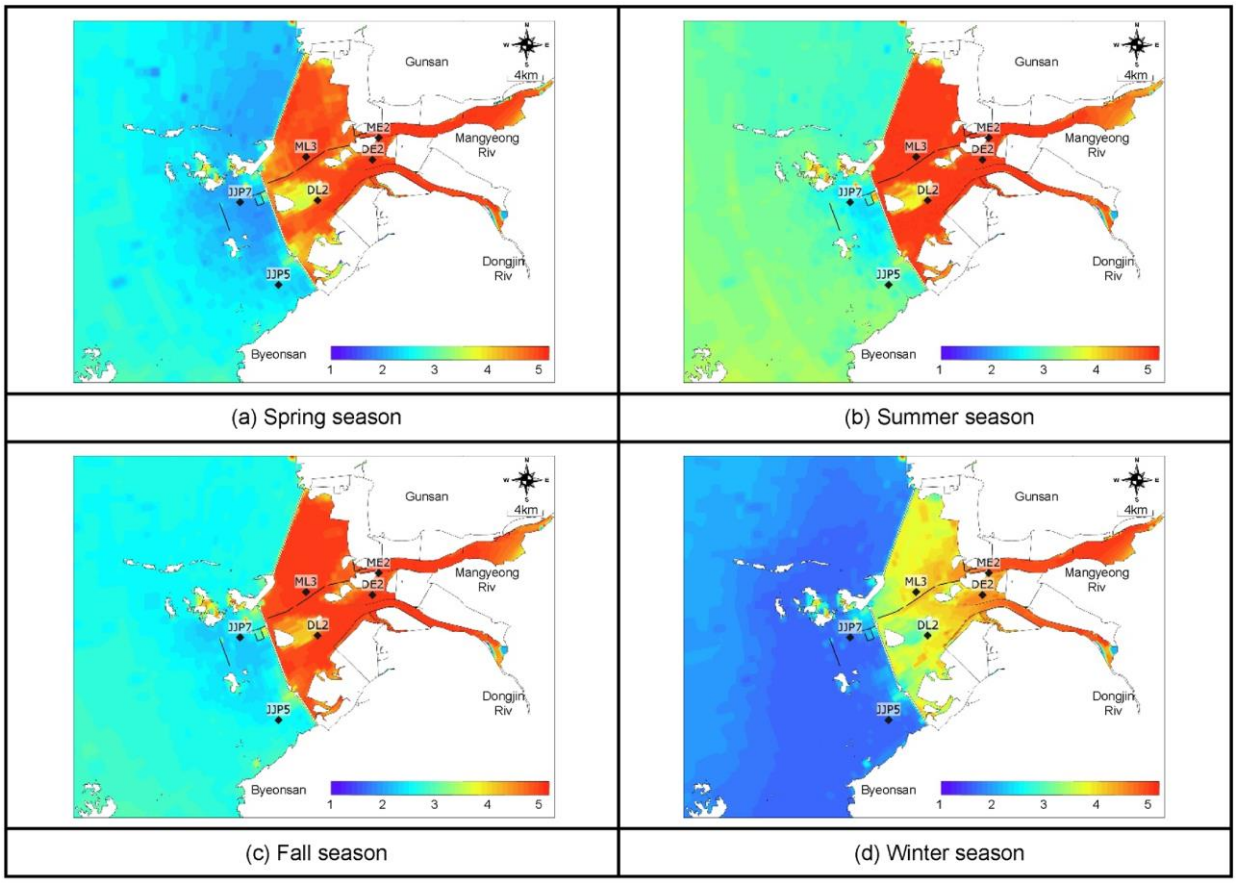

Figure 24. Seasonal distribution of ESWQI (SC-0)

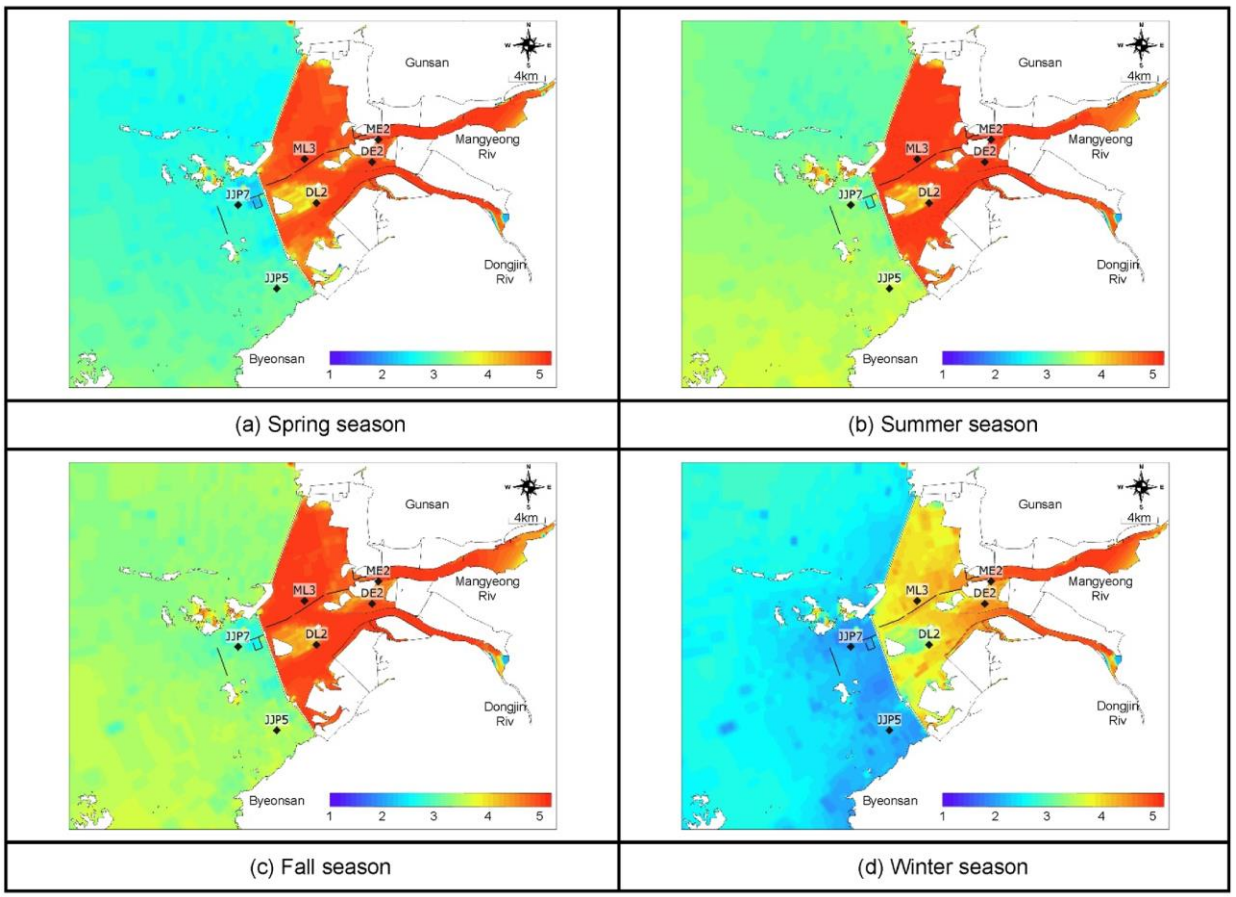

Figure 25. Seasonal distribution of ESWQI (SC-Q1)

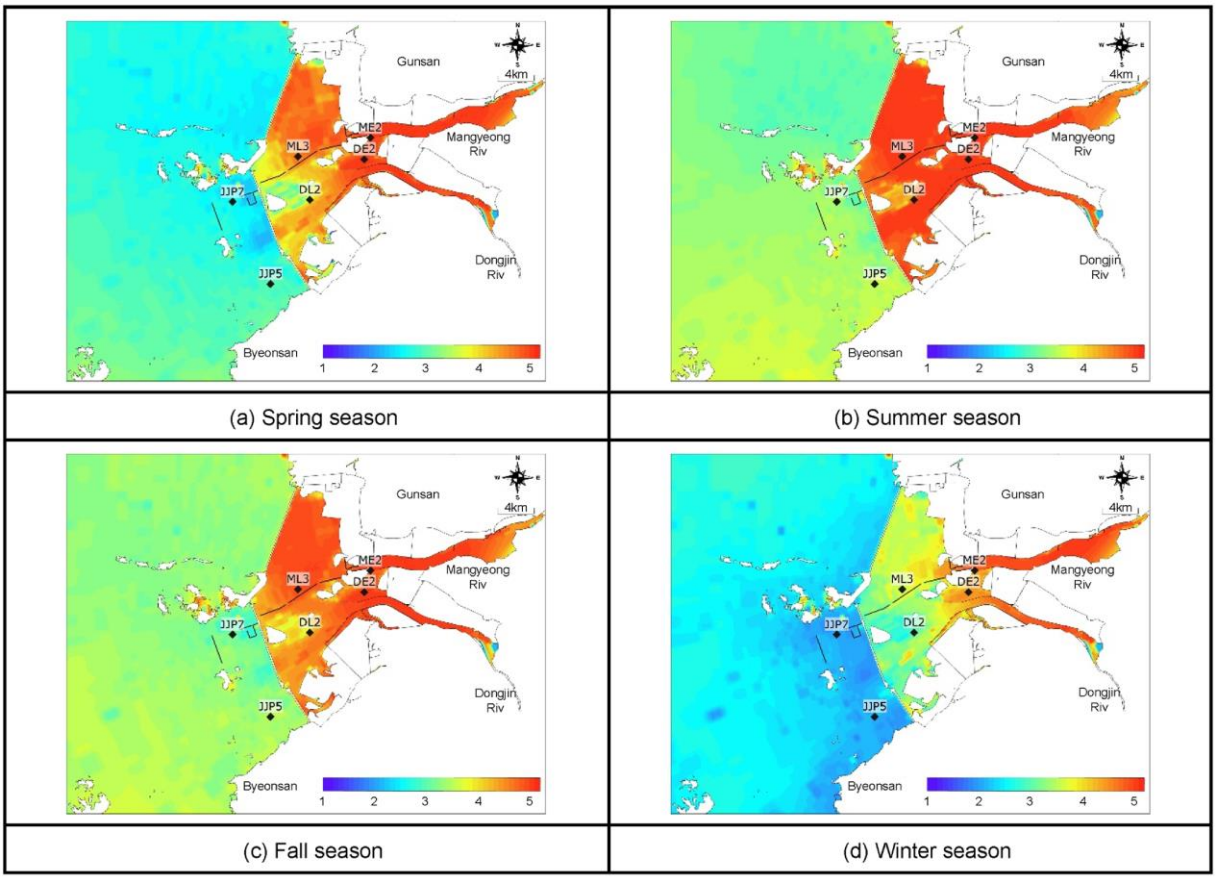

Figure 26. Seasonal distribution of ESWQI (SC-R)

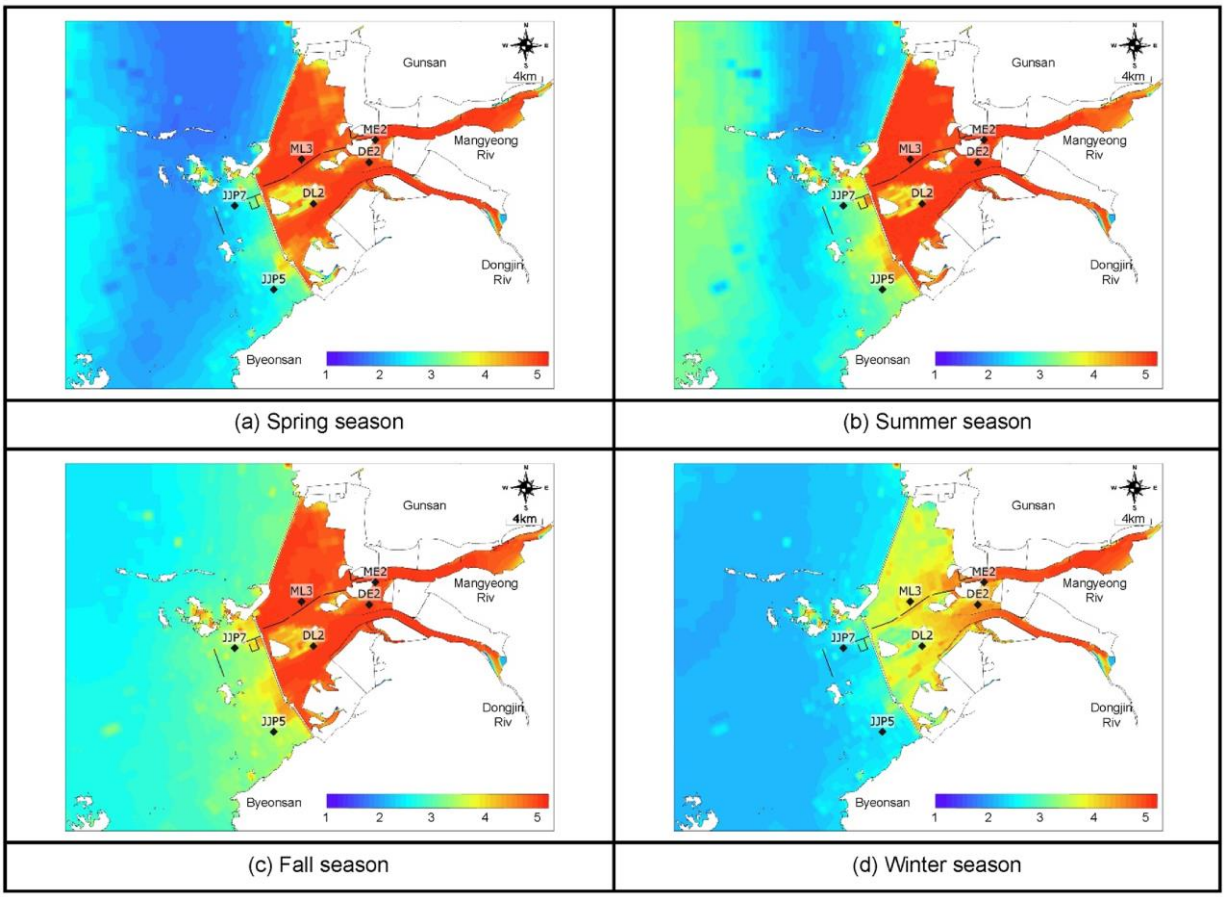

Figure 27. Seasonal distribution of ESWQI (SC-Q2)

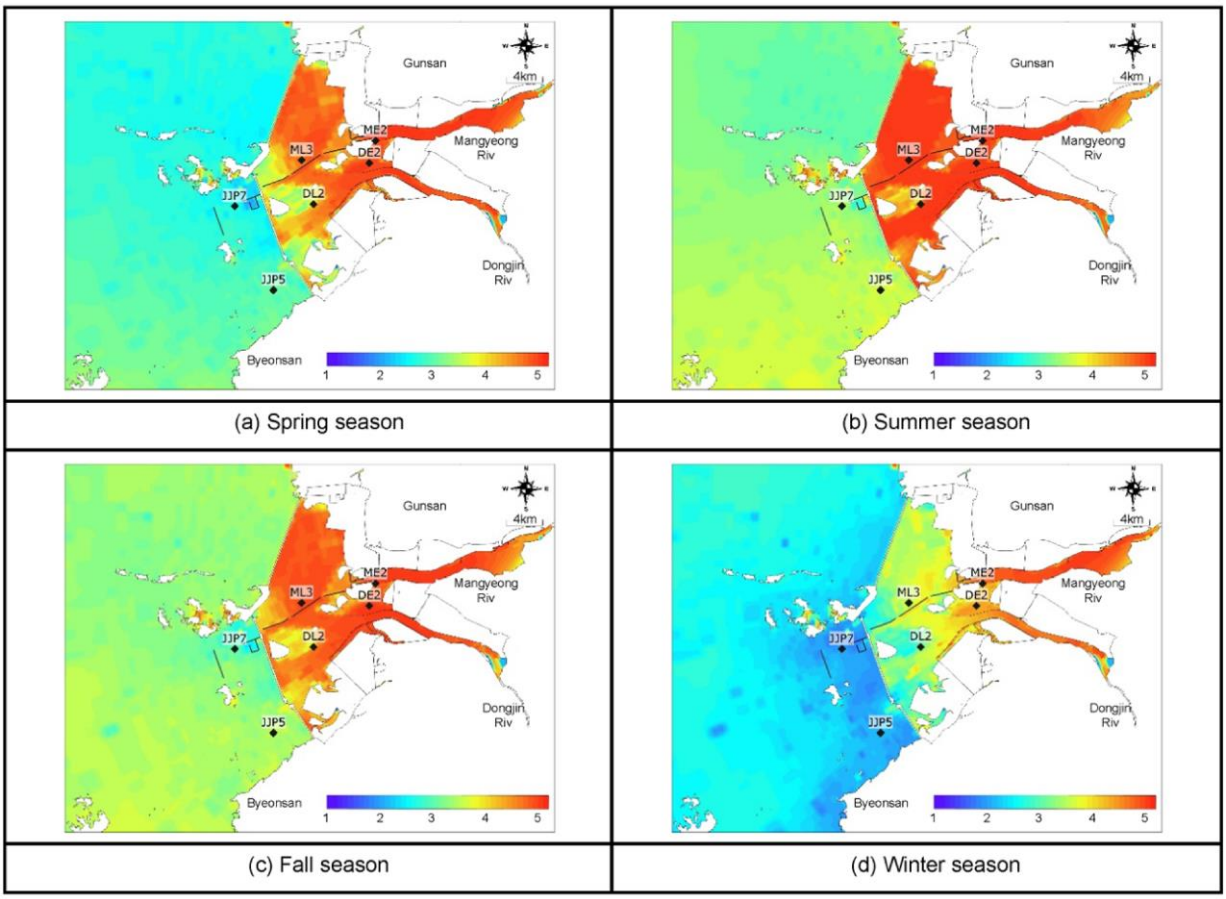

Figure 28. Seasonal distribution of ESWQI (SC-Q3)

The impact of lower layer DO was greater at the ML3 site, where the watershed pollutant load inflow was relatively large, and the water depth was deep. This might be due to the organic matter flowing into the basin consuming a large amount of oxygen during the decomposition process in the lower layer. When the stratification due to salinity is strongly formed and the water layer stability is high, dissolved oxygen cannot be transmitted to the bottom layer. Under these conditions, only dissolved oxygen is consumed for organic matter decomposition, facilitating the formation of a hypoxic water mass. Given the relatively deeper water at point ML3 than point DL2, oxygen transfer would be relatively unfavorable.

SD has a major impact in summer and fall. During the monsoon period, a large amount of rainfall occurs, and the runoff increases, which also increases SS (suspended solid). Therefore, the photosynthesis of phytoplankton may be hindered, and increased pollution prevents light from penetrating the photic layer. DIN, related to eutrophication, exerted a strong effect in spring, while DIP was an influential factor in fall. Given that the Mangyeong River and Dongjin River watersheds are dominated by agricultural land, DIN and DIP likely originate from fertilizers and pesticides [37]. Nutrients such as DIN and DIP affect water quality as retention time increases due to a high nutrient load from nonpoint sources and poor seawater exchange. When excessive nutrients are supplied, the concentrations of DIN and DIP increase, significantly impacting phytoplankton growth. This likely accounts for the relatively high Chl-a concentration. Additionally, excessive phytoplankton growth can cause the sea surface to become turbid, and a hypoxic water mass can form due to the lack of sunlight and oxygen reaching the lower layer of the sea. Similar results were observed when assessing the influence of lower layer DO saturation.

3.5. Evaluation of Variability in Major Water Quality Items

Eutrophication must be considered when managing water quality in lakes. The water quality factors that exert considerable effects on eutrophication include Chl-a, TP, TN, and TOC, which were included in the current study to evaluate water quality variability. The average concentrations were calculated by scenario and major water quality items for ML3 and DL2 stations that represent water quality and ME2 and DE2 stations located upstream. The water quality concentration in the grid was averaged and used to calculate the annual average (Tables 9 and 10). when p-value of 0.05 or greater indicates that the difference in concentration is not statistically significant at the 95% confidence level [67]. The relationships between seawater inflow and major water quality items at the ML3, DL2, ME2, and DE2 stations by scenarios have been illustrated in Figure 30.

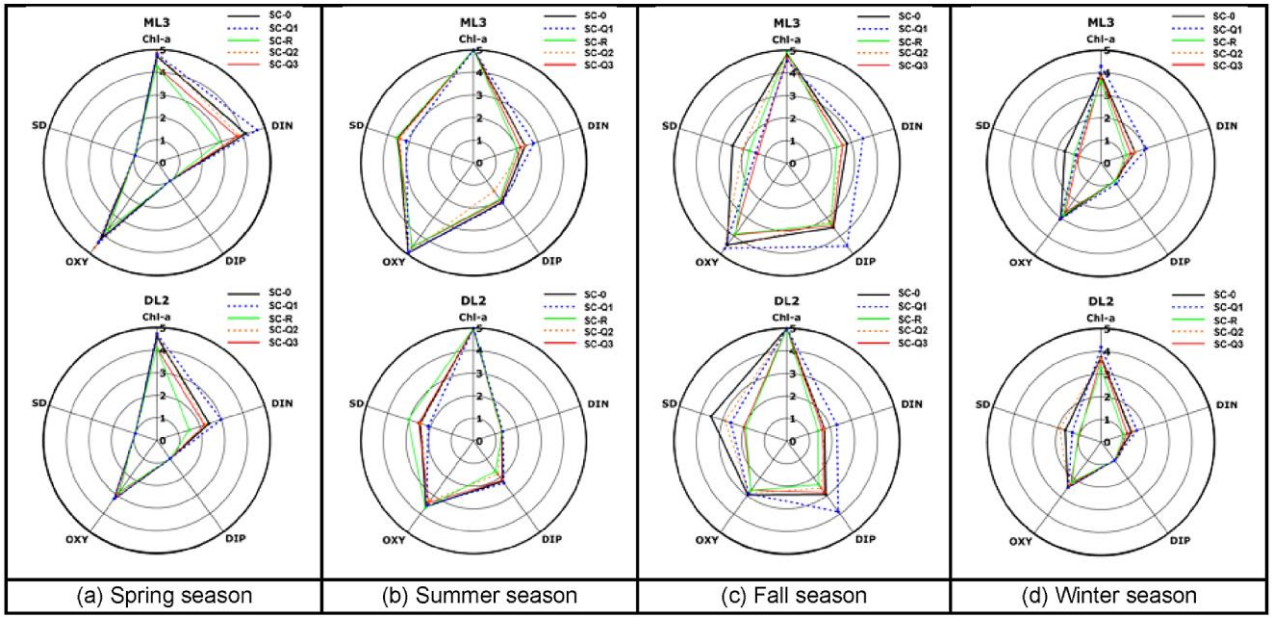

Figure 29. ESWQI distribution and contribution of water quality items by scenario (ML3, DL2)

Table 9. Average annual water quality concentration at ML3 and DL2 stations by scenario

Area	Scenario	TOC (mg/L)		TN (mg/L)		TP (mg/L)		Chl-a (mg/㎥)	
ML3	SC-0	3.03	-	0.72	-	0.047	-	14.06	-
	SC-Q1	3.1	-0.07	0.82	**(0.1)**	0.057	**(0.01)**	12.38	*(-1.68)*
	SC-R	2.97	*(-0.06)*	0.61	*(-0.11)*	0.042	*(-0.005)*	12.53	*(-1.53)*
	SC-Q2	2.96	(-0.07)	0.7	(-0.02)	0.045	(-0.002)	13.1	(-0.96)
	SC-Q3	2.98	(-0.05)	0.67	*(-0.05)*	0.044	(-0.003)	11.5	*(-2.56)*
DL2	SC-0	3.22	-	0.56	-	0.042	-	18.13	-
	SC-Q1	3.31	-0.09	0.66	**(0.1)**	0.051	**(0.009)**	16.54	*(-1.59)*
	SC-R	3.07	*(-0.15)*	0.47	*(-0.09)*	0.035	*(-0.007)*	14.84	*(-3.29)*
	SC-Q2	3.28	-0.06	0.56	0	0.04	(-0.002)	17.76	(-0.37)
	SC-Q3	3.22	0	0.54	*(-0.02)*	0.04	(-0.002)	14.58	*(-3.55)*

The numbers in parentheses represent differences compared to those observed in the SC-0 scenario, with numbers in boldface indicating a decrease in concentration and italics indicating an increase in concentration. The numbers expressed in underline represent results with no statistical significance, indicating no difference noted compared to those in the SC-0 scenario.

Table 10. Average annual water quality concentrations at the ME2 and DE2 stations by scenario

Area	Scenario	TOC (mg/L)		TN (mg/L)		TP (mg/L)		Chl-a (mg/㎥)	
ME2	SC-0	3.87	-	2.08	-	0.079	-	23.55	-
	SC-Q1	3.97	-0.1	2.38	**(0.31)**	0.09	**(0.011)**	18.89	*(-4.66)*
	SC-R	3.96	-0.09	2.25	**(0.17)**	0.083	-0.004	20.48	*(-3.07)*
	SC-Q2	4.15	**(0.28)**	2.4	**(0.33)**	0.079	0	28.38	**(4.83)**
	SC-Q3	3.84	(-0.03)	1.92	*(-0.16)*	0.077	(-0.002)	18.76	*(-4.79)*
DE2	SC-0	3.72	-	1.12	-	0.123	-	13.28	-
	SC-Q1	3.86	-0.14	1.23	**(0.11)**	0.142	**(0.019)**	11.84	*(-1.44)*
	SC-R	3.83	-0.11	1.1	(-0.02)	0.137	**(0.014)**	11.77	*(-1.51)*
	SC-Q2	4.05	**(0.33)**	1.21	**(0.09)**	0.169	**(0.046)**	15.36	**(2.08)**
	SC-Q3	4.18	**(0.46)**	1.04	*(-0.08)*	0.106	*(-0.017)*	12.63	(-0.65)

The numbers in parentheses represent differences compared to those observed in the SC-0 scenario, with numbers in boldface indicating a decrease in concentration and italics indicating an increase in concentration. The numbers expressed in underline represent results with no statistical significance, indicating no difference noted compared to those in the SC-0 scenario.

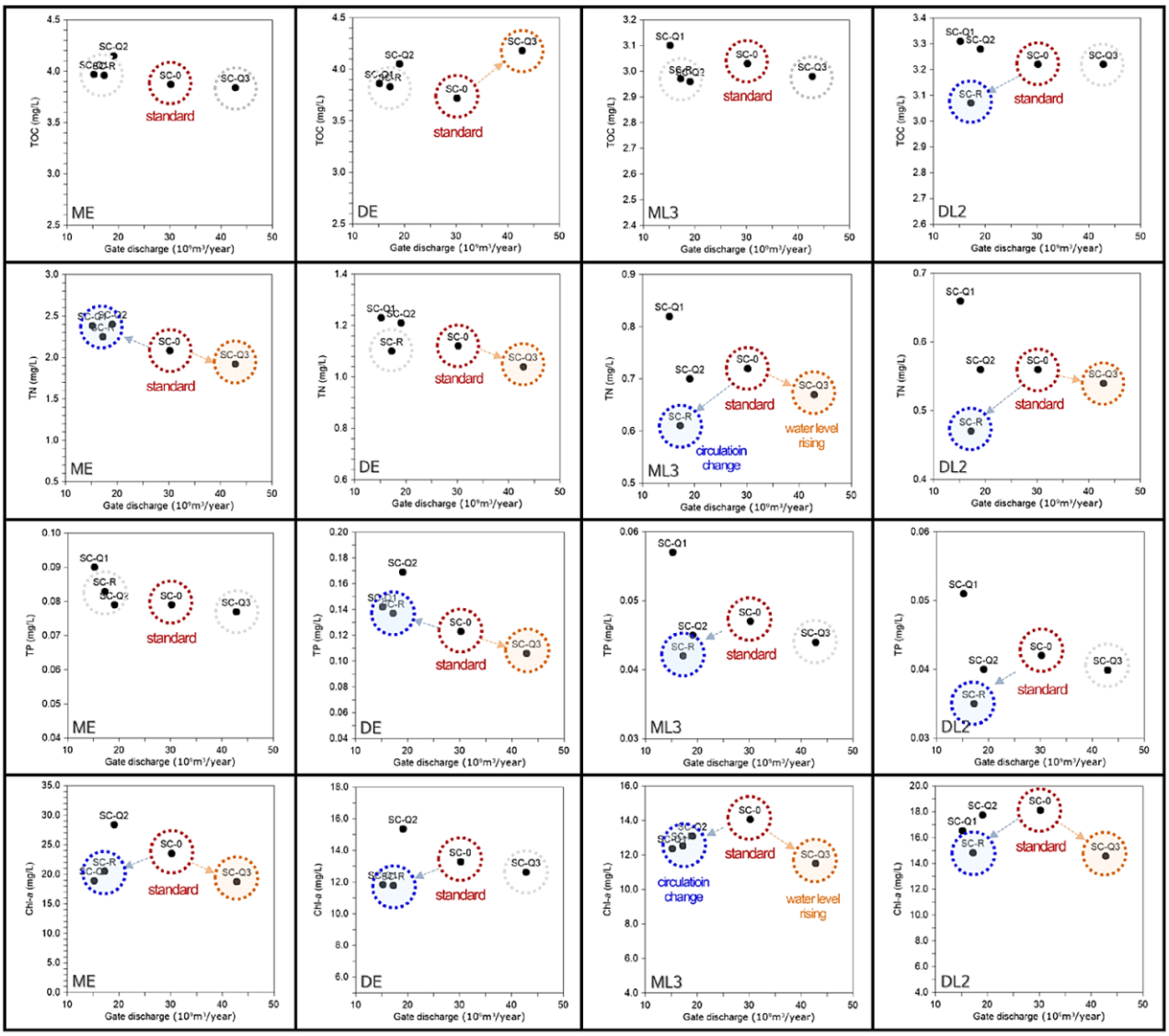

Figure 30. Relationship between seawater inflow and water quality items by scenario

In the SC-0 scenario, the TOC, TN, TP, and Chl-a concentrations were 3.03 mg/L, 0.72 mg/L, 0.047 mg/L, and 14.06 mg/m^3 at the ML3 station; 3.22 mg/L, 0.56 mg/L, 0.042 mg/L, and 18.13 mg/m^3 at the DL2 station; 3.87 mg/L, 2.08 mg/L, 0.079 mg/L, and 23.55 mg/m^3 at the ME2 station; and 3.72 mg/L, 1.12 mg/L, 0.123 mg/L, and 13.28 mg/m^3 at the DE2 station, respectively. In the SC-Q1 scenario, the TN and TP concentrations at the ML3 and DL2 stations exhibited a statistically significant increase compared with the SC-0 scenario, whereas the Chl-a concentration decreased. In the SC-R scenario, the TOC, TN, TP, and Chl-a concentrations at ML3 and DL2 stations exhibited a statistically significant decrease compared with the SC-0 scenario. At the ME2 station, as TN concentration increased, Chl-a concentration significantly decreased. At the DE2 station, the TP concentration was increased, and the Chl-a concentration was significantly decreased. In the SC-Q2 scenario, no statistically significant increases or decreases were noted at the ML3 and DL2 stations; however, all items increased at ME2 and DE2. In the SC-Q3 scenario, TN and Chl-a concentrations significantly decreased at the ML3 and DL2 stations. Moreover, TN and Chl-a concentrations at the ME2 station and TN and TP concentrations at the DE2 station exhibited significant decreases. In the SC-R and SC-Q3 scenarios, improvement in TN, TP, and Chl-a concentrations were observed in most stations. Hence, the scenario with an elevated managed water level (SC-Q3) showed water quality improvement at the ME2 and DE2 stations located upstream of Saemangeum Lake, whereas the scenarios with an altered circulation system (SC-R) and the scenario with elevated managed water level (SC-Q3) showed water quality improvement at the ML3 and DL2 stations located downstream to Saemangeum Lake. Notably, the findings show that in the SC-R scenario, water quality improvement was achieved by effectively using the inflow of seawater despite a 43% decrease in seawater inflow.

In the SC-R scenario, the flux of freshwater flowing from the Mangyeong River and seawater flowing into the Shinsi sluice gate may collide in the water area where the seawater spreads more widely into the lake and moves to the Dongjin water area, improving the low-velocity section and water quality. Meanwhile, the counterclockwise circulation is likely

due to the overall decrease in stagnant water within the lake as the freshwater flowing in from the Dongjin River and the seawater flowing in through the Garyuk sluice gate are circulated through the east–west axis pathway to the Mangyeong water area. Moreover, given that seawater containing a high concentration of dissolved oxygen is rapidly circulated within the lake after flowing in, it can supply dissolved oxygen to the lower layers.

According to the results of Kim et al. [68], in a scenario where the flow in the upper stream of Saemangeum increases by 86% compared to the current state, COD was reduced by 1.3 mg/L, TN by 1.207 mg/L, TP by 0.075 mg/L, and Chl-a by 5.1 mg/L at point M3, and COD was reduced by 0.5 mg/L, TN by 0.205 mg/L, TP by 0.009 mg/L, and Chl-a by 2.1 mg/L at point D3. Points M3 and D3 are upstream of Saemangeum Lake and are similar to points ME2 and DE2 in the current study. However, the Saemangeum basin receives a very high proportion of water from external basins; thus, increasing the water flow internally is limited. Meanwhile, the SC-R scenario of this study showed a positive result in improving water quality even when seawater inflow was reduced by 43% compared with the current state. In the SC-Q3 scenario, this occurrence may be due to the dilution effect of pollutants caused by the increase in the inflow of seawater with good water quality.

4. Conclusion

In this study, a numerical simulation analysis was performed with consideration of non-structural alternatives for improving water quality in Saemangeum Lake. The analysis of the relationships between seawater inflow and water quality items revealed that the volume of seawater inflow for maintaining the target water quality was > 3 × 10^9 t/year and > 0.7 × 10^9 t/month for TOC and > 21.7–23.7 × 10^9 t/year and 1.6–1.8 × 10^9 t/month for TP. Additionally, a large-scale clockwise vortex was formed in the northern part of the Mangyeong area (MK7-ML3 section) and two-layer circulation with different flows in the surface and bottom layers. Importantly, the major water quality items demonstrated a significant improvement at most stations in the scenario in which one-way circulation was alternated in 15-day cycles (SC-R). Water quality improvement was achieved despite a 43% decrease in the annual seawater inflow. In the scenario with an elevated managed water level (SC-Q3), pollutant dilution and water quality improvement were increased due to the large inflow of seawater with good water quality. Hence, for SC-Q3, it is necessary to investigate the impact on flood water levels to ensure flood control stability. Overall, this study's findings will prove valuable in devising engineering solutions to enhance water quality in artificial estuarine lakes.

4.1. Limitations

Due to recent climate change, rainfall intensity is strong and irregular. During the monsoon period, large amounts of river discharge may occur, causing lake water levels to rise rapidly. In particular, during the neap tidal period, the outflow through the sluice gate is limited, which may pose challenges in maintaining flood control within the lake. To mitigate these impacts, a close review of flood control is needed when the management water level is increased step by step. In this analysis, consideration of the worst-case conditions is required, i.e., neap tide period, floods, typhoons, and sea level rise. By combining various conditions, scenarios can be generated, and the associated numerical analysis results can be applied to derive management water levels to ensure flood control and an appropriate water environment. Modeling also faces limitations in accurately simulating turbulent mixing in lakes due to the resolution of numerical grids. While micro-tidal currents can sustain a resuspended state through eddies in fast-flowing waters, hydrostatic models like the Delft3D model encounter challenges in precisely replicating such phenomena. Additionally, the Delft3D model can incorporate general factors limiting algal growth, such as light, water temperature, and nutrients, but is unable to capture physiological algae phenomena (e.g., phosphatase secretion) or direct zooplankton predation. Hence, ensuring reproducibility requires ongoing investigation into input coefficients, calibration/validation data, and updating the model for various hydrologic factors.

5. Declarations

5.1. Data Availability Statement

The data presented in this study are available on request from the corresponding author.

5.2. Funding

The authors received no financial support for the research, authorship, and/or publication of this article.

5.3. Conflicts of Interest

The authors declare no conflict of interest.

6. References

[1] Schubel, J. R., & Carter, H. H. (1984). the Estuary As a Filter for Fine-Grained Suspended Sediment. The Estuary As a Filter, Academic Press, 81-105. doi:10.1016/b978-0-12-405070-9.50011-6.

[2] Morris, A. W. (1985). Estuarine chemistry and general survey strategy. Practical estuarine chemistry: a handbook. Cambridge University Press, Cambridge, United Kingdom.

[3] Jeong, Y. H., & Yang, J. S. (2015). The Long-term Variations of Water Qualities in the Saemangeum Salt-Water Lake after the Sea-dike Construction. Journal of the Korean Society for Marine Environment & Energy, 18(2), 51–63. doi:10.7846/jkosmee.2015.18.2.51.

[4] Lee, C. H., Kang, D. S., Nam, C. H., Lee, B. G., & Ryu, H. G. (2001). Integrated Management Strategies for Estuarine Environments in Korea. Korea Maritime Institute, Seoul, South Korea.

[5] Hirsch, P. E., Schillinger, M., Appoloni, K., Burkhardt-Holm, P., & Weigt, H. (2016). Integrating economic and ecological benchmarking for a sustainable development of hydropower. Sustainability (Switzerland), 8(9), 875. doi:10.3390/su8090875.

[6] Jansky, L., Murakami, M., & Pachova, N. I. (2004). The Danube : Environmental Monitoring of an International River. United Nations University Press, Hong Kong.

[7] McCully, P. (1996). Silenced rivers: the ecology and politics of large dams. International Affairs, 73(4), 799–800. doi:10.2307/2624501.

[8] Guinder, V. A., Popovich, C. A., & Perillo, G. M. E. (2009). Particulate suspended matter concentrations in the Bahía Blanca Estuary, Argentina: Implication for the development of phytoplankton blooms. Estuarine, Coastal and Shelf Science, 85(1), 157–165. doi:10.1016/j.ecss.2009.05.022.

[9] Friedl, G., & Wüest, A. (2002). Disrupting biogeochemical cycles - Consequences of damming. Aquatic Sciences, 64(1), 55–65. doi:10.1007/s00027-002-8054-0.

[10] Baxter, R. M. (1977). Environmental Effects of Dams and Impoundments. Annual Review of Ecology and Systematics, 8(1), 255–283. doi:10.1146/annurev.es.08.110177.001351.

[11] Rosenberg, D. M., Berkes, F., Bodaly, R. A., Hecky, R. E., Kelly, C. A., & Rudd, J. W. M. (1997). Large-scale impacts of hydroelectric development. Environmental Reviews, 5(1), 27–54. doi:10.1139/a97-001.

[12] Luo, X. (2005). Sediment-water flux of hydrophobic organic chemicals due to molecular diffusion and bioturbation. University of California, Santa Barbara, United States.

[13] Różkowski, J., & Rzętała, M. (2021). Uzbekistan's aquatic environment and water management as an area of interest for hydrology and thematic tourism. Journal of Environmental Management and Tourism, 12(3), 642–653. doi:10.14505/jemt.v12.3(51).04.

[14] Bartram, J., & Pedley, S. (1996). Water Quality Monitoring- A Practical Guide to the Design and Implementation of Freshwater Quality Studies and Monitoring Programmes. United Nations Environment Programme; World Health Organization. CRC Press, Florida, United States. doi:10.1002/ejoc.201200111.

[15] Na, E. H., & Park, S. S. (2005). A three-dimensional modeling study of Lake Paldang for spatial and temporal distributions of temperature, current, residence time, and spreading pattern of incoming flows. Journal of Korean Society of Environmental Engineers, 27(9), 978-988.

[16] Kaçikoç, M., & Beyhan, M. (2014). Hydrodynamic and water quality modeling of lake eğirdir. Clean - Soil, Air, Water, 42(11), 1573–1582. doi:10.1002/clen.201300455.

[17] Amorim, L. F., Martins, J. R. S., Nogueira, F. F., Silva, F. P., Duarte, B. P. S., Magalhães, A. A. B., & Vinçon-Leite, B. (2021). Hydrodynamic and ecological 3D modeling in tropical lakes. SN Applied Sciences, 3(4), 444. doi:10.1007/s42452-021-04272-6.

[18] Zheng, X. N., Wu, D. X., Huang, C. Q., Wu, Q. Y., & Guan, Y. T. (2022). Impacts of hydraulic retention time and inflow water quality on algal growth in a shallow lake supplied with reclaimed water. Water Cycle, 3, 71–78. doi:10.1016/j.watcyc.2022.04.004.

[19] Elshemy, M., Khadr, M., Atta, Y., & Ahmed, A. (2016). Hydrodynamic and water quality modeling of Lake Manzala (Egypt) under data scarcity. Environmental Earth Sciences, 75(19), 1329. doi:10.1007/s12665-016-6136-x.

[20] Qin, Z., He, Z., Wu, G., Tang, G., & Wang, Q. (2022). Developing Water-Quality Model for Jingpo Lake Based on EFDC. Water (Switzerland), 14(17), 2596. doi:10.3390/w14172596.

[21] Wu, T., Su, B., Wu, H., Wang, S., Wang, G., Ratnaweera, H., Weerakoon, S. B., Zhang, Z., & Yao, B. (2022). Scenario optimization of water supplement and outflow management in Yilong Lake based on the EFDC model. Hydrology Research, 53(4), 519–531. doi:10.2166/nh.2022.113.

[22] Sarpong, L., Li, Y., Cheng, Y., & Nooni, I. K. (2023). Temporal characteristics and trends of nitrogen loadings in lake Taihu, China and its influencing mechanism at multiple timescales. Journal of Environmental Management, 344, 118406. doi:10.1016/j.jenvman.2023.118406.

[23] Shin, Y. R., Jung, J. Y., Choi, J. H., & Jung, K. W. (2012). Hydrodynamic modeling of Saemangeum reservoir and watershed using HSPF and EFDC. Journal of Korean Society on Water Environment, 28(3), 384-393.

[24] Cho, C. W., Song, Y. S., & Bang, K. Y. (2020). A Study on the Influence of the Saemangeum Sluice-Gates Effluent Discharge using the Particle Tracking Model. Journal of Korean Society of Coastal and Ocean Engineers, 32(4), 211–222. doi:10.9765/kscoe.2020.32.4.211.

[25] Kim, S., & Park, Y. (2023). An Improved Model for Water Quality Management Accounting for the Spatiotemporal Benthic Flux Rate. Water (Switzerland), 15(12), 2219. doi:10.3390/w15122219.

[26] Jung, J., Shin, Y., K, C., Jang, J., & Choi, J. (2011). Application of HSPF-GEMSS Model for Analysis of Salinity in Saemangeum. Korean Studies Information Service System, 176.

[27] Kliem, N., & Pietrzak, J. D. (1999). On the pressure gradient error in sigma coordinate ocean models: A comparison with a laboratory experiment. Journal of Geophysical Research: Oceans, 104(C12), 29781–29799. doi:10.1029/1999jc900188.

[28] Galelli, S., Castelletti, A., & Goedbloed, A. (2015). High-Performance Integrated Control of water quality and quantity in urban water reservoirs. Water Resources Research, 51(11), 9053–9072. doi:10.1002/2015WR017595.

[29] Tabarestani, M. K., & Fouladfar, H. (2022). Effect of reservoir size on water quality in coastal reservoirs during desalinization period using numerical model. Water Supply, 22(5), 5080–5094. doi:10.2166/ws.2022.182.

[30] Shalby, A., Elshemy, M., & Zeidan, B. A. (2020). Assessment of climate change impacts on water quality parameters of Lake Burullus, Egypt. Environmental Science and Pollution Research, 27(26), 32157–32178. doi:10.1007/s11356-019-06105-x.

[31] Wang, N., Chen, Q., Hu, K., Xu, K., Bentley, S. J., & Wang, J. (2023). Morphodynamic modeling of Fourleague Bay in Mississippi River Delta: Sediment fluxes across river-estuary-wetland boundaries. Coastal Engineering, 186, 104399. doi:10.1016/j.coastaleng.2023.104399.

[32] Xu, C., Zhang, J., Bi, X., Xu, Z., He, Y., & Gin, K. Y. H. (2017). Developing an integrated 3D-hydrodynamic and emerging contaminant model for assessing water quality in a Yangtze Estuary Reservoir. Chemosphere, 188, 218–230. doi:10.1016/j.chemosphere.2017.08.121.

[33] Kim, S., Kim, K., & Lee, J. (2023). Real-time WQI Prediction Using AI-based Models. Journal of the Korean Society for Marine Environment & Energy, 26(1), 66–80. doi:10.7846/jkosmee.2023.26.1.66.

[34] Lürling, M., & Mucci, M. (2020). Mitigating eutrophication nuisance: in-lake measures are becoming inevitable in eutrophic waters in the Netherlands. Hydrobiologia, 847(21), 4447–4467. doi:10.1007/s10750-020-04297-9.

[35] Oh, C., Song, Y., Yoon, J.-S., & Jang, J. (2021). A Study on Appropriate Water Quality Management Measures Dependent on a Hydrodynamic Characteristics in Saemangeum Freshening Reservoir. Korea Society of Coastal Disaster Prevention, 8(1), 41–50. doi:10.20481/kscdp.2021.8.1.41.

[36] Choi, H., Kwon, H. I., Yoon, Y. Y., Kim, Y., & Koh, D. C. A preliminary assessment of groundwater chemistry for agricultural water supply in the Mangyeong-Dongjin watershed. Journal of Soil and Groundwater Environment, 26, 65–75. doi:10.7857/JSGE.2021.26.1.065.

[37] Kim, J., Lee, S., Shin, J. Y., Lim, J. H., Na, Y. K., Joo, S., ... & Choi, J. (2018). Effect of Paddy BMPs on Water Quality and Policy Consideration in Saemangeum Watershed. Journal of Wetlands Research, 20(4), 304-313. doi:10.17663/JWR.2018.20.4.304.

[38] MOE. (2024). Ministry of Environment, Seoul, South Korea. Available online: http://www.eariul.go.kr (accessed on December 2024).

[39] MOF. (2024). Ministry of Oceans and Fisheries, Seoul, South Korea. Available online: http://www.meis.go.kr (accessed on December 2024).

[40] KIMST. (2024). Korea Institute of Marine Science & Technology Promotion, Seoul, South Korea. Available online: http://www.kimst.re.kr/ (accessed on December 2024).

[41] KHOA. (2024). Korea Hydrographic and Oceanographic Agency, Seoul, South Korea. Available online: http://www.khoa.go.kr (accessed on December 2024).

[42] Deltares. (2023). 3D-Water Quality: Versatile water quality modelling. Deltares, Delft, Version 1.1 (August 2023). Available online: https://content.oss.deltares.nl/delft3d/D-Water_Quality_User_Manual.pdf (accessed on December 2024).

[43] Deltares. (2024). Delft3D-FLOW, Simulation of Multi-Dimensional Hydrodynamic Flows and Transport Phenomena, Including Sediments. Deltares, Delft, Version 4.05 (August 2024). Available online: https://content.oss.deltares.nl/delft3d4/Delft3D-FLOW_User_Manual.pdf (accessed on December 2024).

[44] Kim, T.-Y., & Yoon, H.-S. (2011). Skill Assessments for Evaluating the Performance of the Hydrodynamic Model. Journal of the Korean Society for Marine Environment & Energy, 14(2), 107–113. doi:10.7846/jkosmee.2011.14.2.107.

[45] Hurley, P. J., Blockley, A., & Rayner, K. (2001). Verification of a prognostic meteorological and air pollution model for year-long predictions in the Kwinana industrial region of Western Australia. Atmospheric Environment, 35(10), 1871–1880. doi:10.1016/S1352-2310(00)00486-6.

[46] D. N. Moriasi, J. G. Arnold, M. W. Van Liew, R. L. Bingner, R. D. Harmel, & T. L. Veith. (2007). Model Evaluation Guidelines for Systematic Quantification of Accuracy in Watershed Simulations. Transactions of the ASABE, 50(3), 885–900. doi:10.13031/2013.23153.

[47] Darwin, C. (1953). Note on hydrodynamics. Mathematical Proceedings of the Cambridge Philosophical Society, 49(2), 342–354. doi:10.1017/S0305004100028449.

[48] Ye, J., & McCorquodale, J. A. (1998). Simulation of Curved Open Channel Flows by 3D Hydrodynamic Model. Journal of Hydraulic Engineering, 124(7), 687–698. doi:10.1061/(asce)0733-9429(1998)124:7(687).

[49] Novak, R. A. (1967). Streamline curvature computing procedures for fluid-flow problems. Journal of Engineering for Gas Turbines and Power, 89(4), 478–490. doi:10.1115/1.3616716.

[50] Constantin, P., Lax, P. D., & Majda, A. (1985). A simple one- dimensional model for the three- dimensional vorticity equation. Communications on Pure and Applied Mathematics, 38(6), 715–724. doi:10.1002/cpa.3160380605.

[51] Zhang, J.-M., Khoo, B. C., Teo, C. P., Haja, N., Tham, T. K., Zhong, L., & Lee, H. P. (2013). Passive and Active Methods for Enhancing Water Quality of Service Reservoir. Journal of Hydraulic Engineering, 139(7), 745–753. doi:10.1061/(asce)hy.1943-7900.0000730.

[52] Park, M. O., Lee, Y. W., Park, J. K., Kang, C. S., Kim, S. G., Kim, S. S., & Lee, S. M. (2019). Evaluation of the seawater quality in the coastal area of Korea in 2013–2017. Journal of the Korean Society for Marine Environment & Energy, 22(1), 47-56. doi:10.7846/jkosmee.2019.22.1.47.

[53] Eaton, J. K., & Fessler, J. R. (1994). Preferential concentration of particles by turbulence. International Journal of Multiphase Flow, 20(SUPPL. 1), 169–209. doi:10.1016/0301-9322(94)90072-8.

[54] Ra, K., Kim, J. K., Kim, E. S., Kim, K. T., Lee, J. M., Kim, S. K., ... & Park, E. J. (2013). Evaluation of spatial and temporal variations of water quality in Lake Shihwa and outer Sea by using water quality index in Korea: A case study of influence of tidal power plant operation. Journal of the Korean Society for Marine Environment & Energy, 16(2), 102-114. doi:10.7846/jkosmee.2013.16.2.102.

[55] Coelho, J. P., Flindt, M. R., Jensen, H. S., Lillebø, A. I., & Pardal, M. A. (2004). Phosphorus speciation and availability in intertidal sediments of a temperate estuary: Relation to eutrophication and annual P-fluxes. Estuarine, Coastal and Shelf Science, 61(4), 583–590. doi:10.1016/j.ecss.2004.07.001.

[56] Hwang, S., Jun, S. M., Song, J. H., Kim, K., Kim, H., & Kang, M. S. (2021). Application of the SWAT-EFDC linkage model for assessing water quality management in an Estuarine reservoir separated by levees. Applied Sciences (Switzerland), 11(9), 3911. doi:10.3390/app11093911.

[57] Welch, E. B., & Patmont, C. R. (1980). Lake restoration by dilution: Moses lake, Washington. Water Research, 14(9), 1317–1325. doi:10.1016/0043-1354(80)90192-X.

[58] Koşucu, M. M., Demirel, M. C., Kirca, V. S. O., & Özger, M. (2019). Hydrodynamic and hydrographic modeling of Istanbul Strait. Processes, 7(10), 710. doi:10.3390/pr7100710.

[59] Cole, T. M., & Wells, S. A. (2006). CE-QUAL-W2: A two-dimensional, laterally averaged, Hydrodynamic and Water Quality Model, Version 3.5. Instruction Report EL-06-1, US Army Engineering and Research Development Center, Vicksburg, United States.

[60] Zison, S. W., Mills, W. B., Deimer, D., & Chen, C. W. (1978). Rates Constants and Kinetics in Surface Water Quality Modeling (First Edition). United States Environmental Protection Agency, EPA-600/3-78-105.

[61] Zison, S., Mills, W., Deimer, D., & Chen, C. (1978). Rates, constants, and kinetics formulations in surface water quality modeling. Final Report, May 1976 - Nov. 1978.

[62] Shimoda, Y., & Arhonditsis, G. B. (2016). Phytoplankton functional type modelling: Running before we can walk? A critical evaluation of the current state of knowledge. Ecological Modelling, 320, 29–43. doi:10.1016/j.ecolmodel.2015.08.029.

[63] Di Maggio, J., Fernández, C., Parodi, E. R., Diaz, M. S., & Estrada, V. (2016). Modeling phytoplankton community in reservoirs. A comparison between taxonomic and functional groups-based models. Journal of Environmental Management, 165, 31–52. doi:10.1016/j.jenvman.2015.08.027.

[64] Pennock, J. R. (1985). Chlorophyll distributions in the Delaware estuary: Regulation by light-limitation. Estuarine, Coastal and Shelf Science, 21(5), 711–725. doi:10.1016/0272-7714(85)90068-X.

[65] Olsson, F., Mackay, E. B., Barker, P., Davies, S., Hall, R., Spears, B., Exley, G., Thackeray, S. J., & Jones, I. D. (2022). Can reductions in water residence time be used to disrupt seasonal stratification and control internal loading in a eutrophic monomictic lake? Journal of Environmental Management, 304, 114169. doi:10.1016/j.jenvman.2021.114169.

[66] Li, J., Li, H., Shen, B., & Li, Y. (2011). Effect of non-point source pollution on water quality of the Weihe River. International Journal of Sediment Research, 26(1), 50–61. doi:10.1016/S1001-6279(11)60075-9.

[67] Cesana, B. M. (2018). What p-value must be used as the Statistical Significance Threshold? P<0.005, P<0.01, P<0.05 or no value at all? Biomedical Journal of Scientific & Technical Research, 6(3), 5310–5318. doi:10.26717/bjstr.2018.06.001359.

[68] Kim, S. M., Park, Y. K., Lee, D. J., & Chung, M. (2017). Prediction of water quality change in Saemangeum reservoir by floodgate operation at upstream. Journal of Korea Water Resources Association, 50(6), 373–386. doi:10.3741/jkwra.2017.50.6.373.

Appendix I

Using ecology-based seawater quality index to improve water quality in an estuarine lake based on sluice gate operation.

Table S1. Annual precipitation analysis for the selection of representative years

Year	Precipitation (mm/year)	Classification	Correlation (R^2)	Percentile (%)
2013	1,164.2	Ordinary year	0.83	34.48
2014	1,196.4	Ordinary year	0.72	41.38
2015	885.9	Low year	0.12	3.45
2016	1,154.3	Ordinary year	0.22	31.03
2017	901.5	Low year	0.90	6.90
2018	1,403.3	Ordinary year	0.77	58.62
2019	1,053.0	Low year	0.54	20.69
2020	1,735.1	Abundant year	0.94	96.55
2021	1,355.7	Ordinary year	0.87	55.17
2022	1166.6	Ordinary year	0.69	27.59

R^2: Correlation between 30-year average monthly precipitation and monthly precipitation.

%: Percentile of 30-year precipitation.

Table S2. Standards for each evaluation item of ESWQI

Score	Chl-*a*	DO Saturation of the lower layer	Epilimnion DIN	Epilimnion DIP	Transparency
	$(\mu g/L)$	(%)	$(\mu g/L)$	$(\mu g/L)$	(m)
1	2.2	90	425	30	1
2	2.42	81	467.5	33	0.9
3	2.75	67.5	531.25	37.5	0.75
4	3.3	45	637.5	45	0.5
5	3.3	45	637.5	45	0.5

Table S3. ESWQI criteria

Grade	Marine Environment Management Act	Sea Environment Standards		
	ESWQI (Score)	COD (mg/L)	TN (mg/L)	TP (mg/L)
I	23 or less	1 or less	0.3 or less	0.03 or less
II	24-33 or less	2 or less	0.6 or less	0.05 or less
III	34-46 or less			
IV	47-59 or less	4 or less	1.0 or less	0.09 or less
V (Other than grade)	60 or more	Exceeds 4	Exceeds 1.0	Exceeds 0.09

Table S4. Capacity by water level and seawater inflow by water level drawdown (management water EL of -1.5 m)

Water EL (m)	Water volume (10^6 m^3)	Water volume ratio by management water level (%)	Water volume deviation (10^6 m^3)	Inflow water volume ratio by management water level (%)
-1.5	1,217	100.00%	-	-
-1.7	1,174	96.40%	44	3.60%
-2.0	1,110	91.20%	107	8.80%

Table S5. Capacity by water level and seawater inflow by water level drawdown (management water EL of -1.3 m)

Water EL (m)	Water volume (10^6 m^3)	Water volume ratio by management water level (%)	Water volume deviation (10^6 m^3)	Inflow water volume ratio by management water level (%)
-1.3	1,262	100.0%	-	-
-1.5	1,217	96.5%	44	0.0%
-1.7	1,174	93.0%	88	3.5%
-2.0	1,110	88.0%	152	7.0%

Table S6. Capacity by water level and seawater inflow by water level drawdown (management water EL of -1.7 m)

Water EL (m)	Water volume (10^6 m^3)	Water volume ratio by management water level (%)	Water volume deviation (10^6 m^3)	Inflow water volume ratio by management water level (%)
-1.7	100.0%	0.0%	-	-
-2.0	94.6%	5.4%	64	5.4%

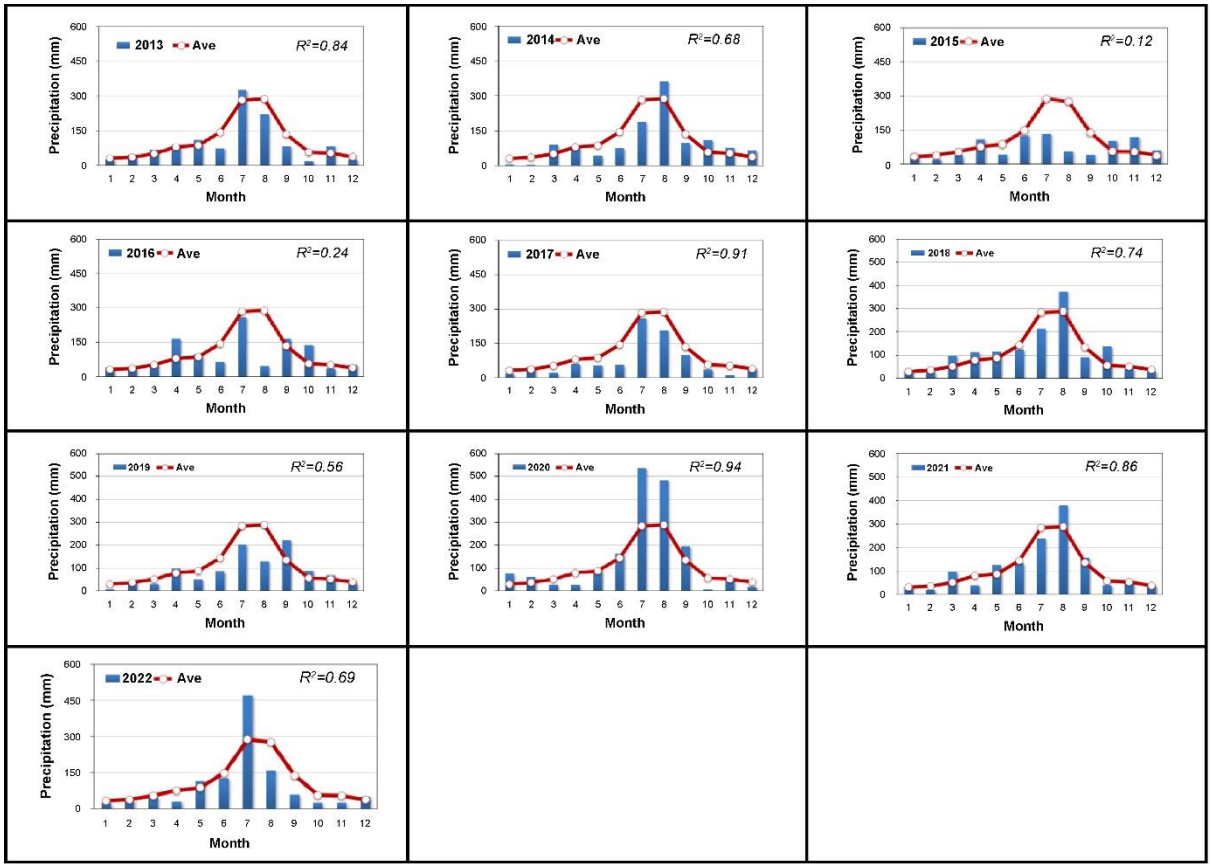

Figure S1. Monthly precipitation by year

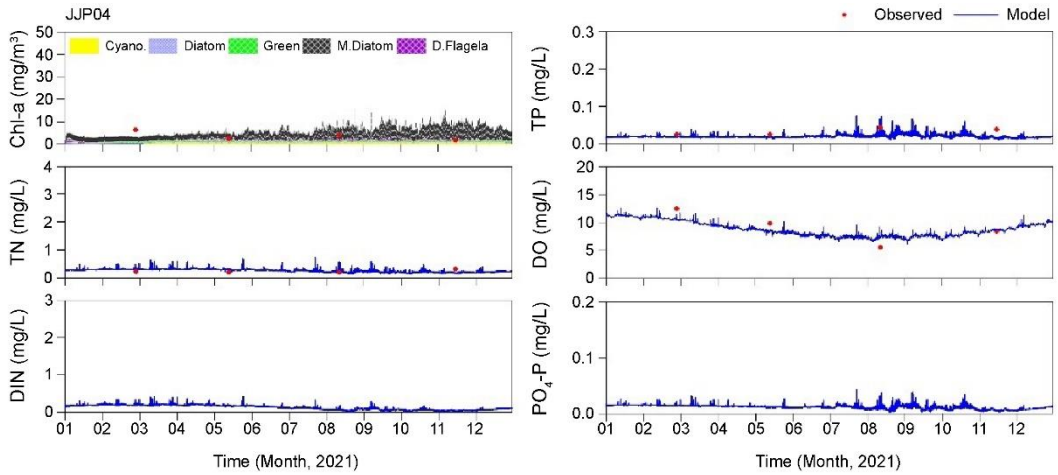

Figure S2. Comparison of observed and simulated water quality time series at point JJP4

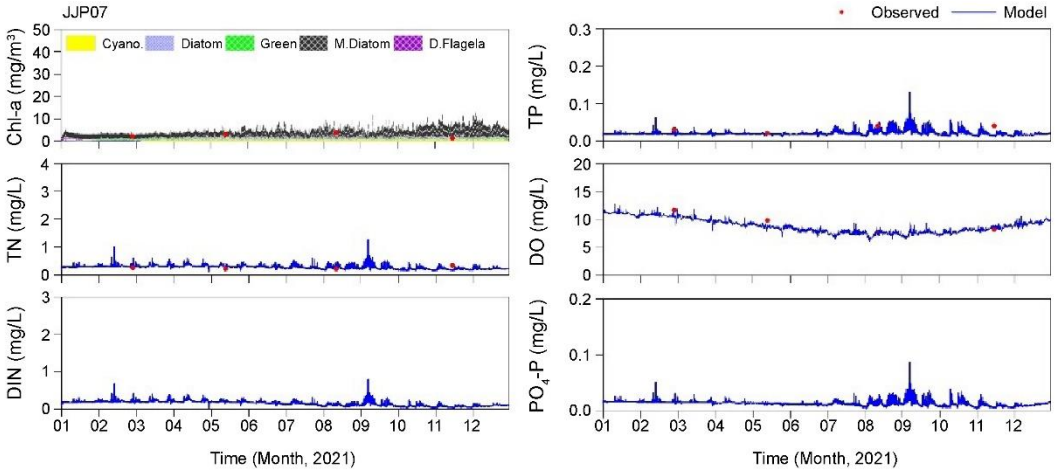

Figure S2. Comparison of observed and simulated water quality time series at point JJP7

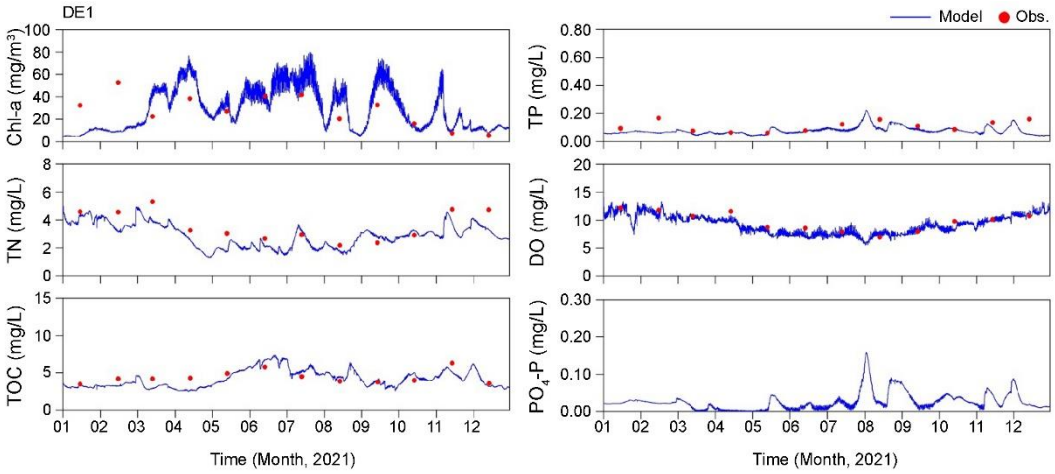

Figure S3. Comparison of the observed and simulated water quality time series at point DE1

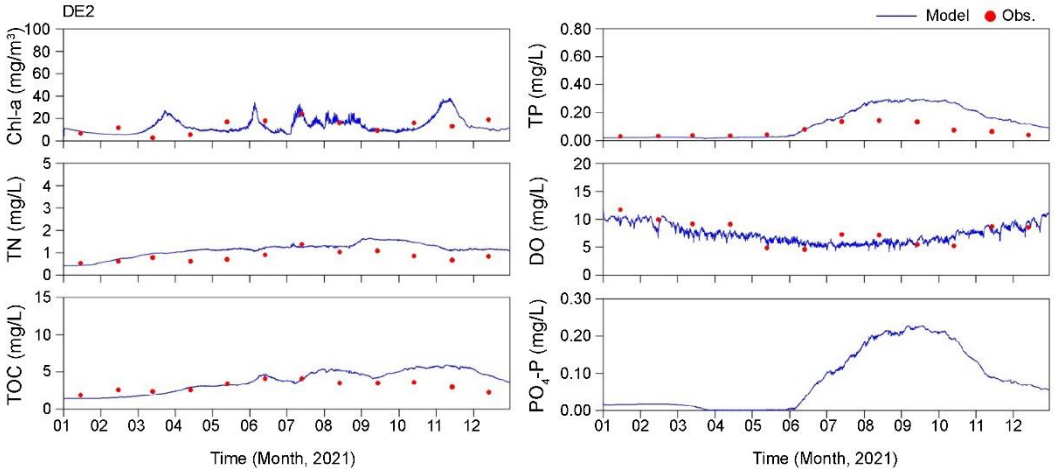

Fig S4. Comparison of the observed and simulated water quality time series at point DE2

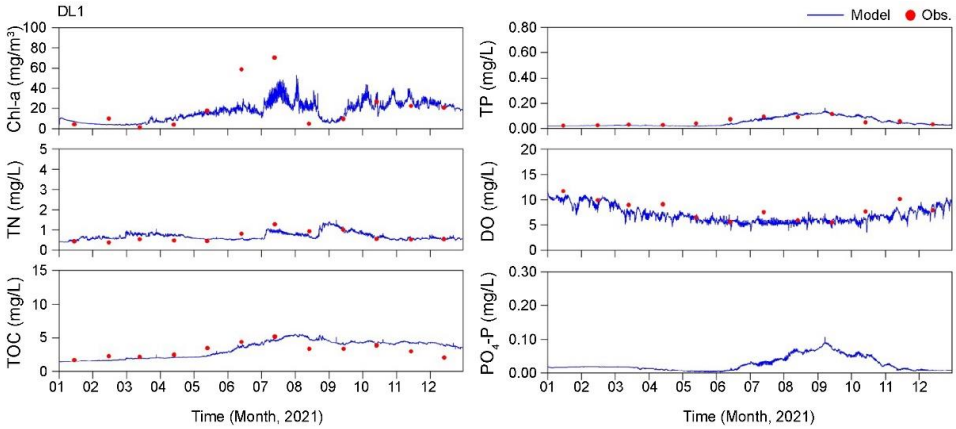

Figure S5. Comparison of the observed and simulated water quality time series at point DL1

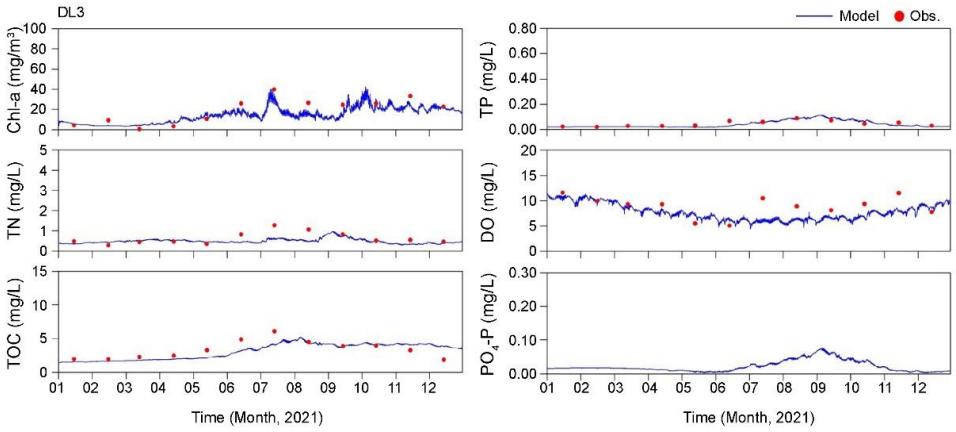

Figure S6. Comparison of the observed and simulated water quality time series at point DL3

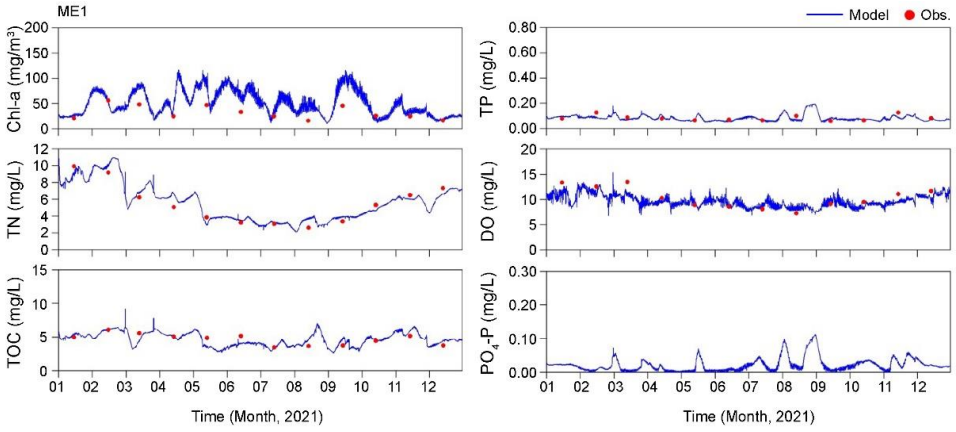

Figure S7. Comparison of the observed and simulated water quality time series at point ME1

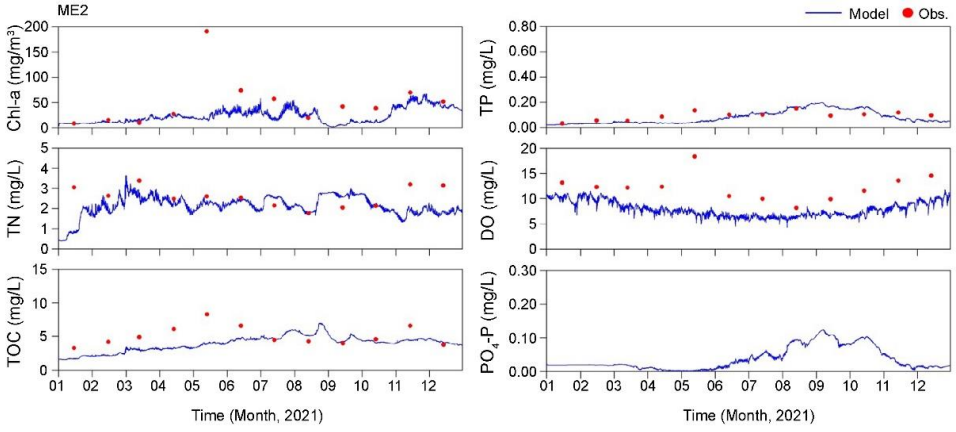

Figure S8. Comparison of the observed and simulated water quality time series at point ME2

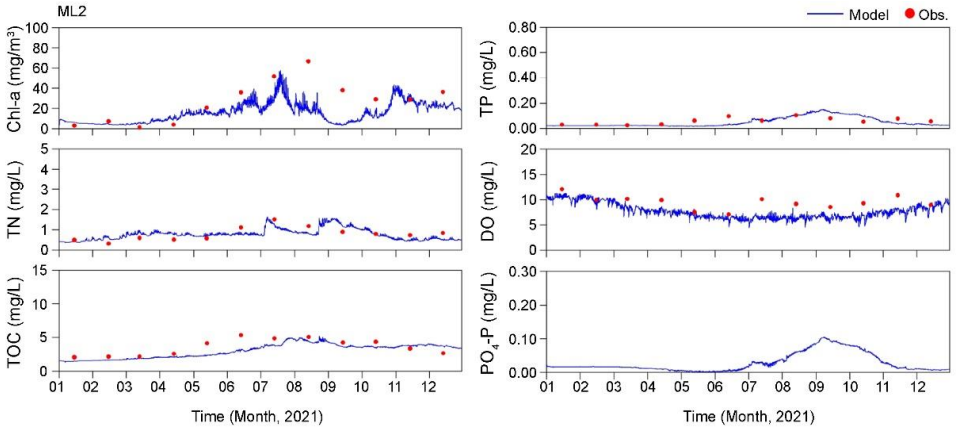

Figure S9. Comparison of the observed and simulated water quality time series at point ML2

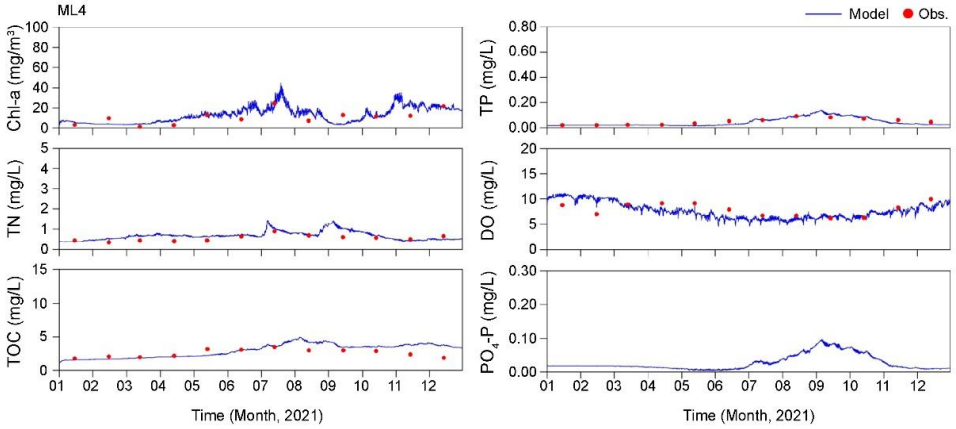

Figure S10. Comparison of the observed and simulated water quality time series at point ML4

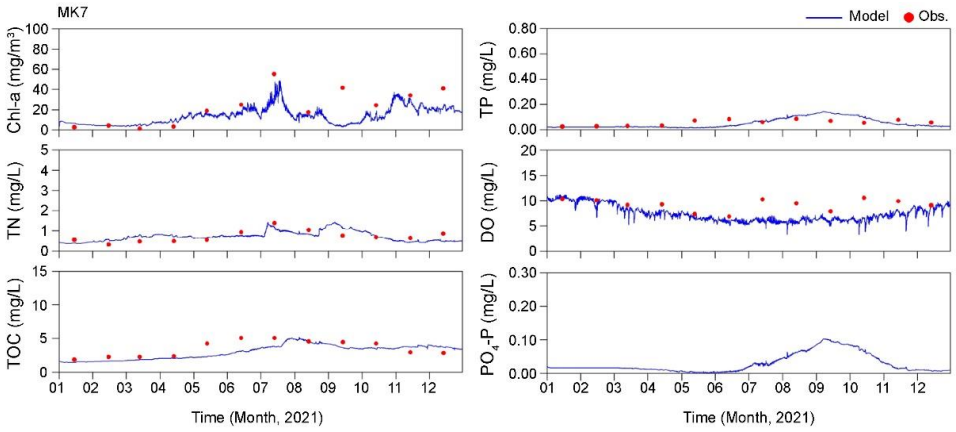

Figure S11. Comparison of observed and simulated water quality time series at point MK7

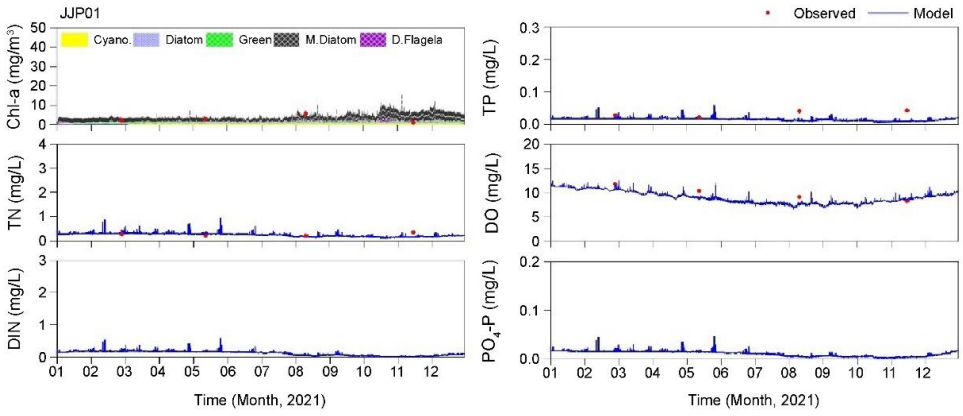

Figure S12. Comparison of the observed and simulated water quality time series at point JJP1

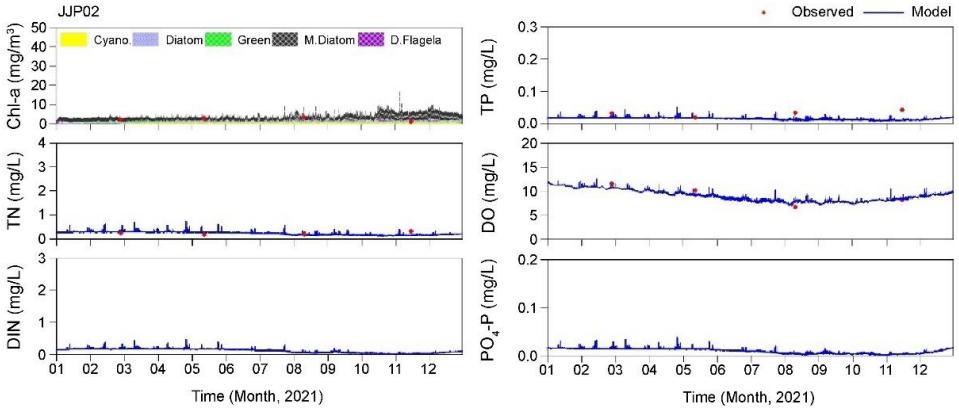

Figure S13. Comparison of the observed and simulated water quality time series at point JJP2

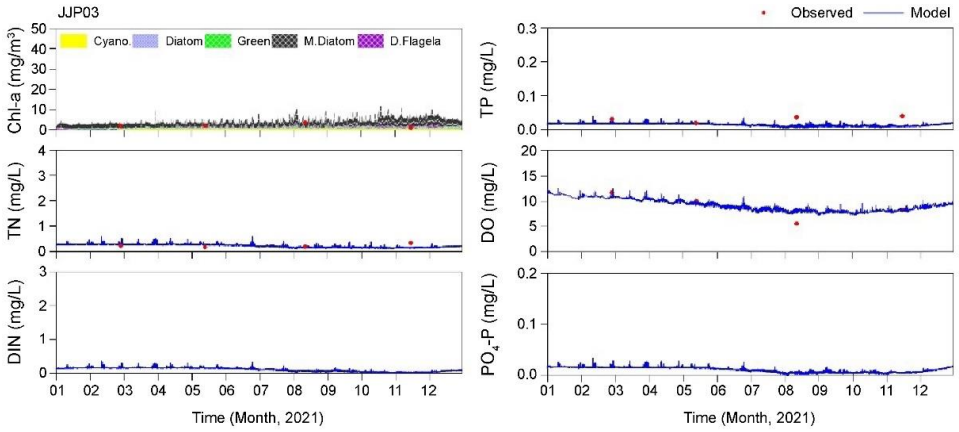

Figure S14. Comparison of the observed and simulated water quality time series at point JJP3

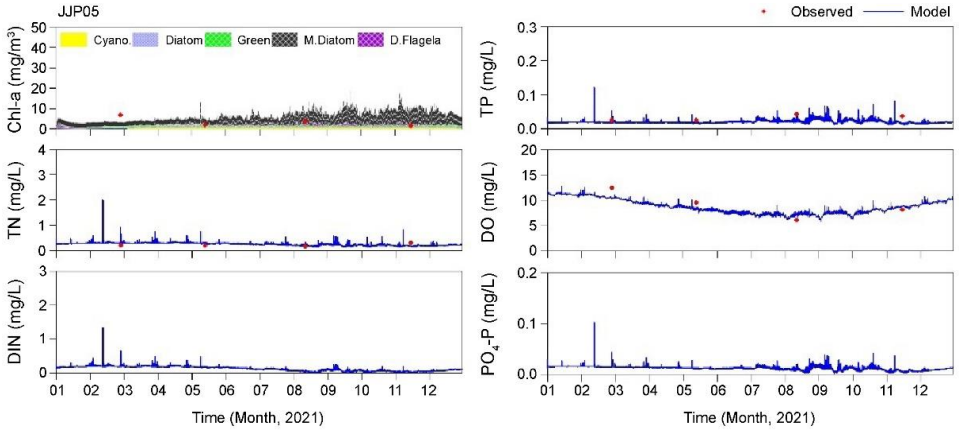

Figure S15. Comparison of the observed and simulated water quality time series at point JJP5

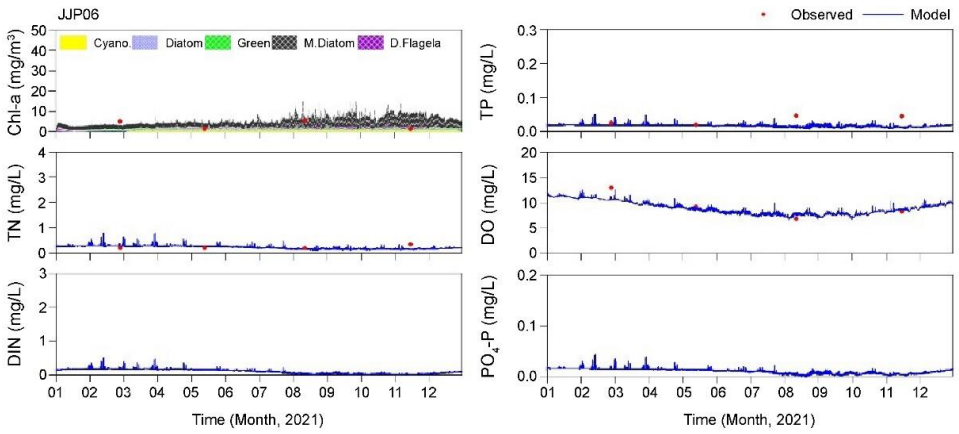

Figure S16. Comparison of the observed and simulated water quality time series at point JJP6

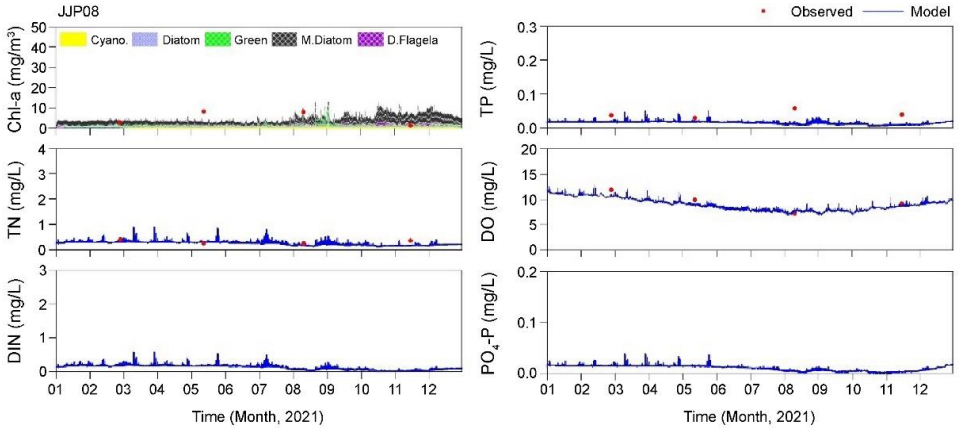

Figure S17. Comparison of observed and simulated water quality time series at point JJP8

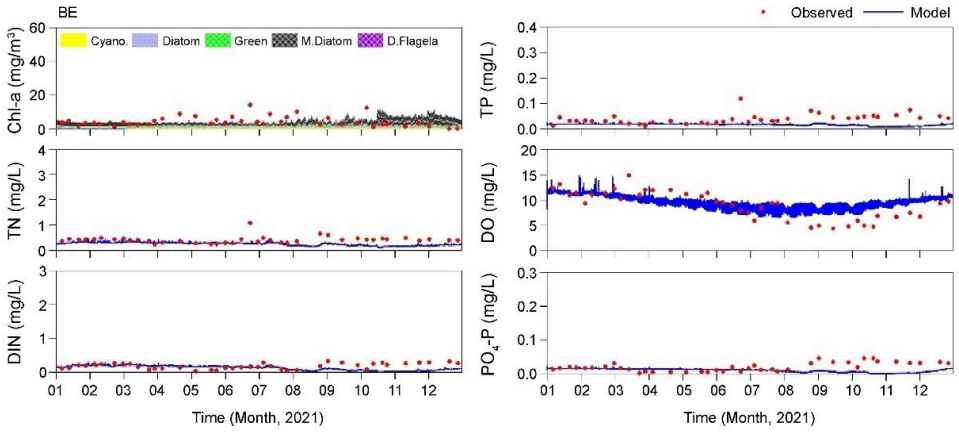

Figure S18. Comparison of the observed and simulated water quality time series at point BE

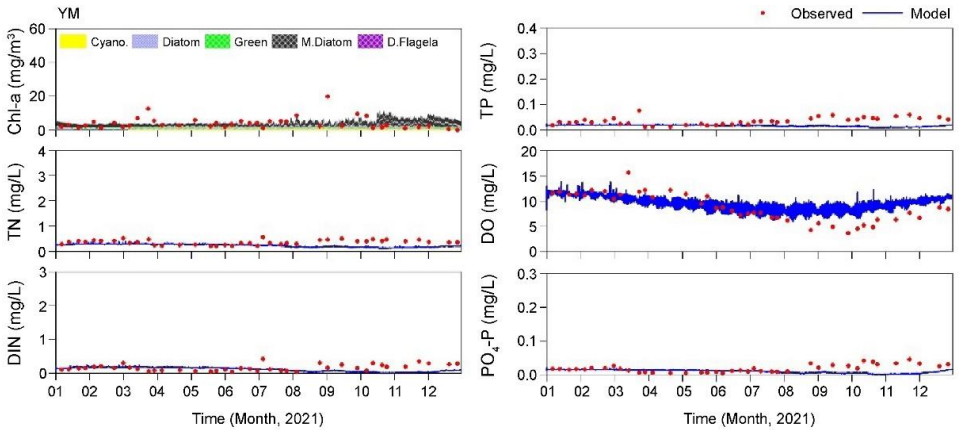

Figure S19. Comparison of the observed and simulated water quality time series at point YM

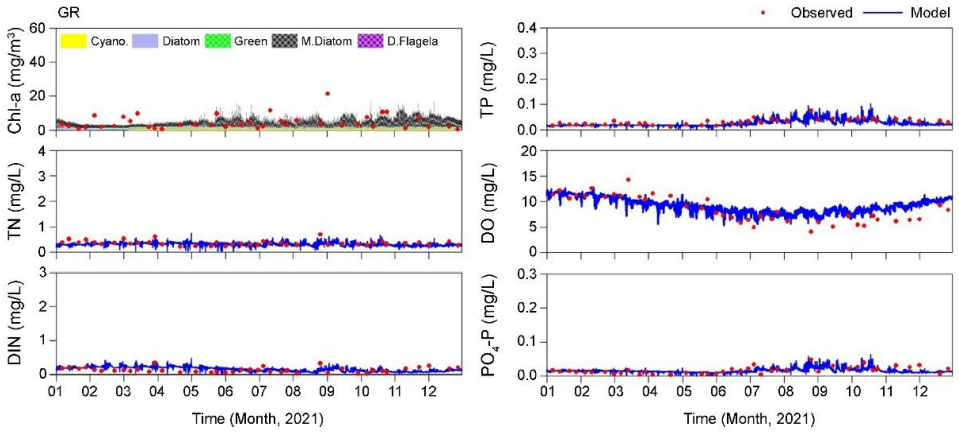

Figure S20. Comparison of the observed and simulated water quality time series at point GR